Lighting the Way: Computations of Stable Forms of Optical Lift

---

A Thesis
Presented to
The Division of Mathematics and Natural Sciences
Reed College

In Partial Fulfillment
of the Requirements for the Degree
Bachelor of Arts

Robby Gottesman

May 2017

Approved for the Division
(Physics)

Lucas Illing

Acknowledgements

With little regard for brevity, I want to thank quite a few people.

To my great friends at Reed and abroad: Forrest, Ahyan, Akanksha, Elias, Alex, Hulali, Mina, Bobby, Collin, and JJ thank you for your help through times both good and bad.

To my fellow thesising seniors, especially Yuka and Edgar, thank you for suffering and laughing with me.

To Lucas, you're the best thesis adviser I've ever had! I don't think I can express how much you've taught me in an entire book, not to mention this sentence.

Shout out to Nancy Gottesman!

Table of Contents

Introduction **1**

Chapter 1: Background **3**
1.1 Optical Momentum 3
1.2 Radiation Pressure & Optical Forces 4
1.2.1 Optical Momentum in a Material 5
1.2.2 Optical Ray Momentum 9
1.2.3 Radiation Pressure with Transmission 10

Chapter 2: Modeling Optical Wings **17**
2.1 Ray Tracing Procedure 19
2.1.1 Defining Rays and Surfaces 20
2.1.2 Finding Ray Intersections 21
2.1.3 Determining $\hat{n}$ 23
2.1.4 Reflection 23
2.1.5 Transmission 26
2.1.6 Optical Forces 31
2.2 Reflective Semicylinder 31

Chapter 3: Results **45**
3.1 Torque and Forces 45
3.1.1 Dynamics 49

Future Work **53**

Appendix A: Mathematica Code **55**
A.1 Generate Rays 55
A.2 Find Intersection between Ray and Surface 56
A.3 Change in Direction for Reflected and Transmitted Ray 57
A.4 Force of Rays on Surface 59
A.5 Extra Information 60

Appendix B: Center of Mass of a Semicylinder **61**

Appendix C: Moment of Inertia of a Semicylinder **63**

References **65**

List of Tables

3.1 Stable angles of attack for refractive semicylinders 46

List of Figures

1.1 Demonstration of illumination area with oblique incidence 6
1.2 Power and intensity of a plane wave 10
1.3 Description of optical rays 11
1.4 Ray diagram demonstrating transmission and reflection of an incident ray 12

2.1 Demonstration of optical lift 19
2.2 Visualization of the components of rays normal to and tangential to an interface 24
2.3 Ray diagram with total internal reflection 28
2.4 Demonstration of Ray tracing algorithm's visual output 32
2.5 Reflective semicylinder in an unrotated configuration 33
2.6 Reflective semicylinder that is rotated an angle ω 36
2.7 A reflective semicylinder undergoing a $\omega > \frac{\pi}{2}$ rotation 38
2.8 The magnitude of the torque in the $\hat{z}$ direction vs. ω for a reflective semicylinder 41
2.9 Topmost and bottommost rays generated for a semicylinder 42
2.10 Comparison of analytic and numeric results 44

3.1 Torque vs. angle of rotation for refractive semicylinders 47
3.2 Visualizations of refractive hemicylinders at their stable angles of attack 48
3.3 Numeric calculations of the angle of rotation of semicylinders as a function of time 50
3.4 $\vec{F} \cdot \hat{y}$ vs. n for a transparent semicylinder 52

Abstract

An optical ray tracing module was developed in *Mathematica* to characterize the efficiency of optical wing designs. This procedure calculates the optical forces and resulting torque on a homogenous, transparent body with constant index of refraction and finds whether the body experiences stable angles of attack and lift forces. We analytically determine the forces and torque on a flat mirror and reflective half cylinder and find excellent agreement with the results of the numeric procedure. Finally, the dynamics of a half-cylindrical wing is modeled.

Introduction

The usage of light as a medium to remotely exert forces on physical objects is not a new idea. In 1871, physicists James Clerk Maxwell and Adolfo Bartoli [1] asserted that electromagnetic waves contain an intrinsic momentum density, and, thus, can exert forces on physical bodies. However, the radiation pressure on a solid body wasn't experimentally demonstrated until 1899 by Pyotr Lebedev [2]. Since then, optical forces were found to have an important influence on planetary formation [3] (see Poynting-Robertson effect), space travel [4], and has even found a use in engineering [5]. Despite knowledge of optical momentum and radiation pressure for nearly a century and a half, it was only in 2010 that a research group led by Grover Swartzlander at the Rochester Institute of technology discovered that certain dielectric surfaces can interact with light such that they can generate optical forces orthogonal to the light's original direction of propagation [6]. This effect is the main focus of this thesis.

Swartzlander et al. termed the orthogonal force "optical lift" [6] after the analogous lift force in aerodynamics. The apparent similarities in the optical forces on the dielectric surface and the aerodynamic forces on an airfoil lead to these surfaces to be called optical wings or lightfoils. The more surprising discovery is that the optical forces would, at certain angles of attack, result in a stable configuration. These optical wings would rotate into a stable angle of attack and maintain that orientation. Beforehand, it hadn't occurred to anyone to treat refractive objects as a lightfoil (analogous to an airfoil). Nearly all previous treatment of radiation pressure only involved reflection and absorption; ignoring the possible effect of refraction, which is

required for stable optical lift.

In short, this thesis attempts to generate a ray-tracing module that can accommodate any dielectric surface and determine its utility as a lightfoil. For the purpose of this thesis, an effective optical wing will exhibit at least one stable orientation and generate a non-zero lift force at that orientation. We construct an optical wing surface with analytically-solvable optical forces and torques in order to generate an intuition about what constitutes an effective lightfoil. Finally, we'll compare the results of our example cases to the numerically-derived results of the ray tracing module.

Chapter 1

Background

1.1 Optical Momentum

In classical electrodynamics, oscillating electromagnetic fields have an intrinsic energy and momentum density. The ability of an electromagnetic wave to transport energy to a physical object is described by its Poynting vector, $\vec{S}$. In vacuum,

$$\vec{S} = \frac{1}{\mu_0}(\vec{E} \times \vec{B}), \tag{1.1}$$

where μ_0 is the permeability of free space, $\vec{E}$ is the vector describing the electric field, and $\vec{B}$ is the vector describing the magnetic field. In simple terms, $\vec{S}$ is the energy per unit time, transported through a unit area by the field. The momentum density, $\vec{g}$, of an electromagnetic field is [7]

$$\vec{g} = \mu_0\epsilon_0\vec{S} = \epsilon_0(\vec{E} \times \vec{B}). \tag{1.2}$$

Consequently, the momentum stored in a field is the volume integral of Eq. 1.2,

$$\vec{p} = \mu_0\epsilon_0 \int_\nu \vec{S}\, dV. \tag{1.3}$$

1.2 Radiation Pressure & Optical Forces

Since the electromagnetic fields contain momentum, they have the capacity to impart momentum to physical objects, and thus exert a force on a solid body. It is important to note that $\vec{S}$ is not constant. For a plane wave, $\vec{S} \propto \cos^2(f\ t)$, where f is proportional to the frequency of $\vec{E}$ and $\vec{B}$. Since the period of visible light is so brief, ($\approx 10^{-15}$ sec), any practical measurement of the momentum of a field will inherently contain many cycles of an electromagnetic field and so one takes the time average of the Poynting vector over a cycle with period T. The time average of the Poynting vector is

$$\langle \vec{S} \rangle = \frac{1}{T} \int_0^T \vec{S} dt, \tag{1.4}$$

$\langle \vec{S} \rangle$ is the average power per unit area transported by an oscillating electromagnetic field; called the intensity, I, of the field.

For a monochromatic plane wave propagating in the $\hat{z}$ direction, the time average of the Poynting vector, $\langle \vec{S} \rangle$, and momentum density, $\langle \vec{g} \rangle$ are

$$\langle \vec{S} \rangle = I = \frac{1}{2}\ c\epsilon_0 E_0^2 \hat{z}, \tag{1.5}$$

$$\langle \vec{g} \rangle = \frac{1}{2\ c}\ \epsilon_0 E_0^2 \hat{z}. \tag{1.6}$$

If we let this plane wave fall at normal incidence on a perfectly absorbing body, then all of the field's momentum will be deposited to the body. In a time Δt, the momentum transfered is [7]

$$\Delta p = |\langle \vec{g} \rangle|\ A\ c\ \Delta t$$

where A is the area of the body illuminated by the plane wave. We can now define the **radiation pressure**, P, as the average force per unit area on the body,

$$P_{absorb} = \frac{1}{A}\frac{\Delta p}{\Delta t} = \frac{1}{2}\epsilon_0 E_0^2 = \frac{I}{c}. \tag{1.7}$$

If we let the body be perfectly reflective, then the radiation pressure will be doubled over the perfectly absorptive case,

$$P_{reflect} = 2\frac{I}{c}. \tag{1.8}$$

Since Eqs. 1.7 & 1.8 are only valid if the plane wave falls at normal incidence on the surface, we need to extend the equations to be more general. Consider a plane wave that falls on the body at some angle α. Then, a smaller component of the momentum of the field will change direction after interacting with the body and the area illuminated will be decreased. Both of these effects will contribute a coefficient of $\cos\alpha$ to Eqs. 1.7 & 1.8. A visualization of this is given in Fig 1.1. With this in mind, the radiation pressure by absorption and reflection are

$$P_{absorb} = \frac{I}{c}\cos^2\alpha \tag{1.9}$$

and

$$P_{reflect} = 2\,\frac{I}{c}\cos^2\alpha, \tag{1.10}$$

respectively. We've shown that EM fields both contain momentum and must exert forces on solid surfaces. Given a perfectly reflective or absorbing body, one can use Eqs. 1.9 & 1.10 to find the radiation pressure on the object. However, this cozy picture is complicated when we allow light to transmit into the body.

1.2.1 Optical Momentum in a Material

There are conflicting choices concerning the momentum of an electromagnetic field in a material with refractive index n. The choice stems from the fact that there are at least two interpretations of the Poynting vector. The first, named after 20th century

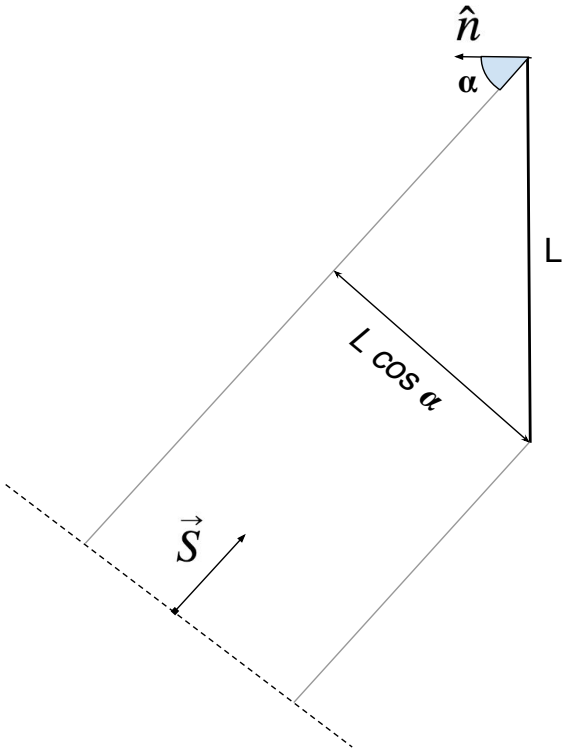

Figure 1.1: A plane wave with Poynting vector $\vec{S}$ and a physical body of length L with normal vector $\hat{n}$ are depicted. The angle α denotes the angle between $\vec{S}$ and $\hat{n}$. As α increases, the frontal surface area illuminated by the plane wave is decreased by a factor of $\cos\alpha$

physicist Hermann Minkowski, says that the Poynting vector, $\vec{S}_{Mink}$, is

$$\vec{S}_{Mink} = \frac{1}{\mu_0\ \epsilon_0}\vec{D} \times \vec{B} \tag{1.11}$$

where $\vec{D}$ is the electric displacement field. This equation is contrasted with the Abraham interpretation, named after Physicist Max Abraham, which instructs us that the Poynting vector, $\vec{S}_{Abr}$, is

$$\vec{S}_{Abr} = \vec{E} \times \vec{H}. \tag{1.12}$$

It's important to note that $\vec{S}_{Mink}$ and $\vec{S}_{Abr}$ both simplify to Eq. 1.1 in a vacuum. However, if we consider a field inside of a nonmagnetic ($\vec{B} = \mu_0 \vec{H}$), dielectric material, then

$$\vec{D} = \epsilon_0 \epsilon_{mat} \vec{E},$$

where ϵ_{mat} is the relative permittivity of the material, and

$$n = \sqrt{\epsilon_{mat}}.$$

Substituting $\vec{D}$ and n into Eqs. 1.11 & 1.12,

$$\vec{S}_{Mink,mat} = \frac{\epsilon_{mat}}{\mu_0} \vec{E} \times \vec{B} = n^2 \vec{S}_{vac} \tag{1.13}$$

and

$$\vec{S}_{Abr,mat} = \vec{S}_{vac}, \tag{1.14}$$

where $\vec{S}_{vac}$ is the Poynting vector in vaccuum as given by Eq. 1.1. From Eq. 1.2, we can define momentum densities $\vec{g}_{Mink}$ and $\vec{g}_{Abr}$ in a material based upon $\vec{S}_{Mink,mat}$ and $\vec{S}_{Abr,mat}$ as

$$\vec{g}_{Mink} = n^2 \ \vec{g}_{vac}$$

and

$$\vec{g}_{Abr} = \vec{g}_{vac},$$

respectively.

Consider a field traveling through a material with index of refraction n. The momentum, $\vec{p}$, in a designated portion of the field is

$$\vec{p} = \vec{g} \ V,$$

where V is the volume of the portion of the field we're considering and $\vec{g}$ is the momentum density using either the Abraham or Minkowski interpretation. The field momentum flowing through an area, A, in a time dt is

$$\vec{p} = \vec{g} \cdot A \; vdt$$

where v, the velocity of the field, is $v = \frac{c}{n}$. Substituting in $\vec{g}_{Mink}$ for $\vec{g}$ yields

$$\vec{p}_{Mink} = n^2 \; \frac{\vec{E} \times \vec{B}}{\mu_0 \; c^2} \frac{c}{n} \; A \; dt$$

$$\vec{p}_{Mink} = n \; \vec{p}_{vac}. \tag{1.15}$$

and substituting in $\vec{g}_{Abr}$ gives

$$\vec{p}_{Abr} = \frac{\vec{E} \times \vec{B}}{\mu_0 \; c^2} \frac{c}{n} \; A \; dt$$

$$\vec{p}_{Abr} = \frac{\vec{p}_{vac}}{n} \tag{1.16}$$

In both cases, p_{vac} is the momentum of the field if it were in a vacuum [8]. The Minkowski and Abraham equations were derived nearly a century ago (1908 and 1909, respectively), and it seems that both are correct [8, 9]. Under certain experimental conditions, the Minkowski momentum will seem correct and the Abraham momentum will seem correct under different condition. For example, if a fluid is set in motion by an optical force, the Abraham momentum is determined to be the correct one [6, 9]. This leaves us with a dilemma; how can we know the optical force on a transparent solid body? Since our derivation of the optical force on a body in Eqs. 1.7 - 1.10 is based on the principle of conservation of momentum, we require insight into whether $\vec{p}_M$ or $\vec{p}_A$ is the correct equation to apply to our particular system.

1.2.2 Optical Ray Momentum

Since depicting the reflection and transmission of wavefronts at a curved dielectric isn't trivial, we will approximate a given electromagnetic field with optical rays. An optical ray is a straight line that is drawn to represent the direction of flow of energy of the field [4]. More specifically, for a given point in space, the ray will point in the direction of the field's Poynting vector at that point. This definition requires that the ray is always pointing perpendicular to the wavefront. The main reason we transition to using a ray interpretation is due to the ease of finding the effect of a dielectric interface on the electromagnetic field (See Eq. 1.20 & 1.21).

Consider a plane wave moving in the $\hat{z}$ direction with intensity I. Let's now focus on a section of this plane wave in the x-y plane of area $\mathcal{A}$. In this case, the power, Φ, flowing through this area is

$$\Phi = I\mathcal{A} \tag{1.17}$$

Now, let's propagate N evenly spaced rays from this area (Fig. 1.3). In this case, the power carried by each ray will be

$$\Phi_{ray} = \frac{I\mathcal{A}}{N} \tag{1.18}$$

. Since depicting a wavefront isn't practical for transmission events, we will use rays as an analogue.

From Eq. 1.7 - 1.10, the radiation pressure on a surface is proportional to $\frac{I}{c}$ for a plane wave. Since rays are of infinitesimal thickness, if we decompose the plane wave into a number of rays, then it seems like the idea of radiation pressure to be unsuitable to the ray description of fields. However, there is no real problem as the ray is only an approximation of the power flowing through a finite area (see Fig 1.3). In decomposing the field into rays, we have simply compressed the power from a finite area into a point. The momentum flowing through the surface $\mathcal{A}$ in a time Δt is (see

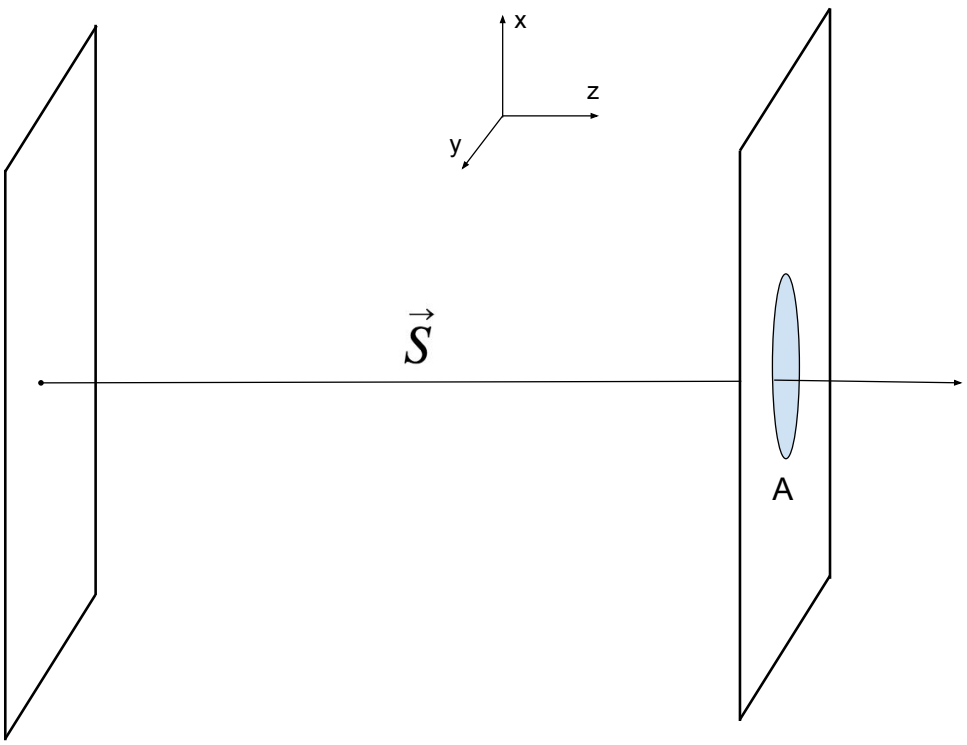

Figure 1.2: A plane wave with intensity I and Poynting vector $\vec{S}$ directed in the $\hat{z}$ direction is depicted. The power flowing through an area $\mathcal{A}$ in the x-y plane is $\Phi = I\mathcal{A}$

Eqs. 1.5 & 1.6)

$$\Delta p = \frac{I}{c}\mathcal{A}\ \Delta t.$$

For N rays evenly spaced over this surface, the momentum flowing through a single ray in a time Δt is

$$\Delta\vec{p}_{ray} = \frac{1}{N}\frac{\langle\vec{S}\rangle}{c}\mathcal{A}\Delta t = \frac{\Phi_{ray}}{c}\ \Delta t\ \hat{z}. \tag{1.19}$$

Note that $\Phi_{ray}\Delta t$ is just the total energy flowing through the ray in a time Δt.

1.2.3 Radiation Pressure with Transmission

Let's now imagine a dielectric interface between two materials with index of refraction n_1 and n_2. If we project an incident ray of light, denoted by **I**, at this interface, then we expect two new rays, the transmitted ray, **T**, and the reflected ray, **R**, to be

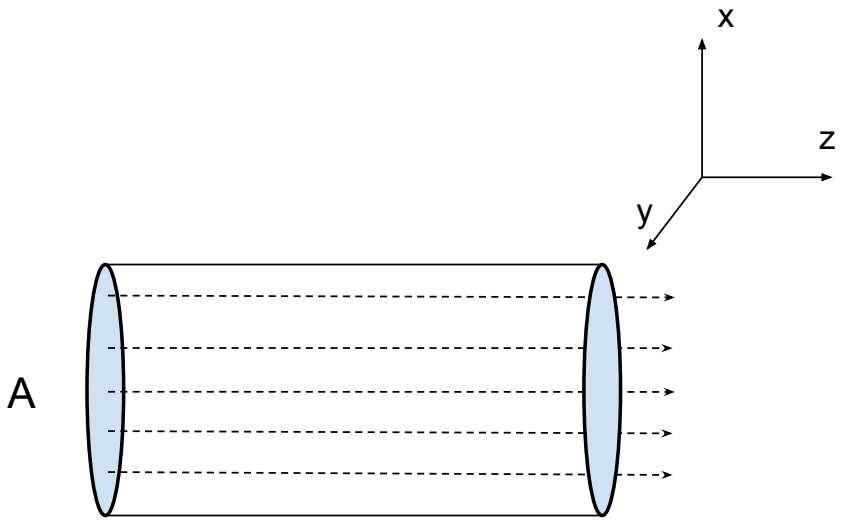

Figure 1.3: A number of rays are propagated from the area $\mathcal{A}$ shown in Fig. 1.2. If the power passing through the area is Φ, then each ray will have a power $\Phi_{ray} = \frac{\Phi}{N}$, where N is the number of rays.

generated where the incident ray intersects the interface. Given that the incident ray has some angle, θ_i, with respect to the normal of the interface, we can find the direction of the reflected and transmitted ray using the law of reflection

$$\theta_i = \theta_r, \tag{1.20}$$

and Snell's law

$$n_2 \sin\theta_t = n_1 \sin\theta_i, \tag{1.21}$$

with θ_r being the angle between the normal and the reflected ray and θ_t the angle between the transmitted ray and normal. Let $\vec{p_i}$ be the momentum of the incident ray of light and $\vec{p_r}$ and $\vec{p_t}$ be the momentum of the reflected and transmitted ray,

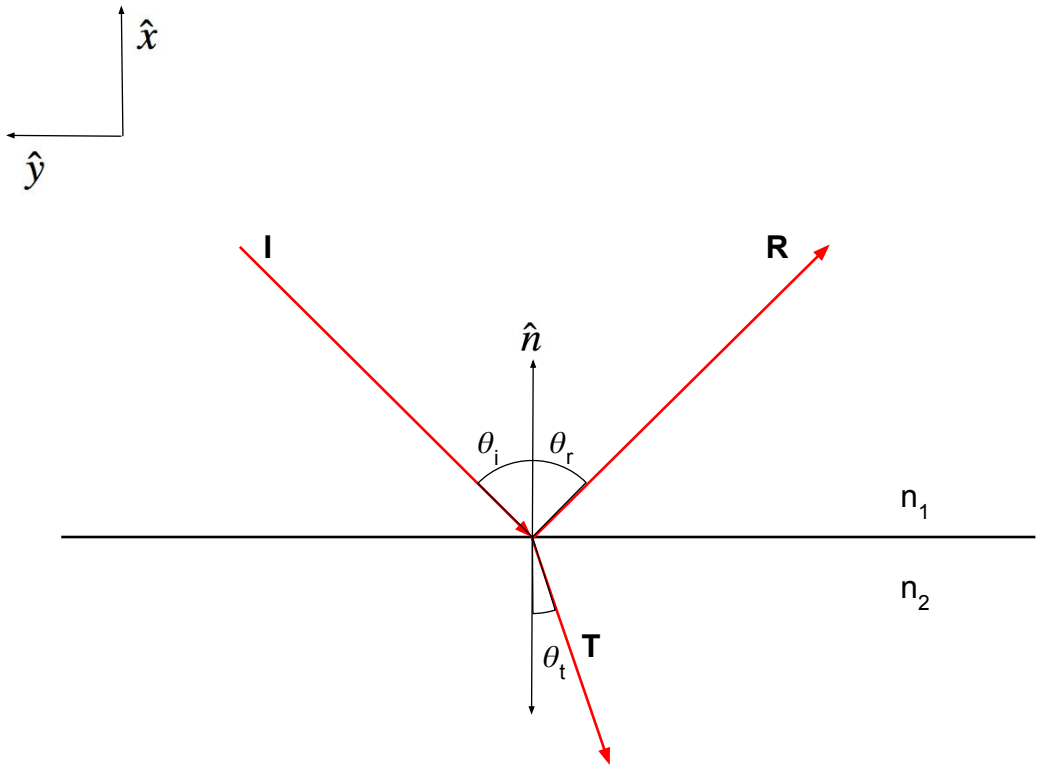

Figure 1.4: An incident ray, I, reflected ray, R, and transmitted ray, T, and their angles θ_i, θ_r, and θ_t relative to the normal of a dielectric interface.

respectively. From conservation of momentum, $\vec{p}_{initial} = \vec{p}_{final}$, we obtain

$$\vec{p}_i = \vec{p}_r + \vec{p}_t + \vec{p}_{mechanical} \tag{1.22}$$

where $\vec{p}_{mechanical}$ is the momentum of the refractive body after the incident ray interacts with the body. If we orient the axes as shown in Fig. 1.4, then Eq. 1.22 can be rewritten as

$$\vec{p}_{mechanical} = \vec{p}_i - \vec{p}_r - \vec{p}_t$$

$$\vec{p}_{mechanical} = |p_i| \begin{pmatrix} -\cos\theta_i \\ -\sin\theta_i \end{pmatrix} - |p_r| \begin{pmatrix} \cos\theta_r \\ -\sin\theta_r \end{pmatrix} - |p_t| \begin{pmatrix} -\cos\theta_t \\ -\sin\theta_t \end{pmatrix} \tag{1.23}$$

where $|\vec{p}_i|$, $|\vec{p}_r|$, and $|\vec{p}_t|$ is the magnitude of the rays' momentum vectors. In order to continue, we need some way to determine $|\vec{p}_r|$ and $|\vec{p}_t|$ as a function of $|\vec{p}_i|$.

The Reflectance, R, and Transmittance, T, of a field determines the intensity of the reflected and transmitted portions of an electromagnetic field at a dielectric interface. Formally, if an incident field has an intensity of I_0, then

$$R = \frac{I_r}{I_0} \tag{1.24}$$

and

$$T = \frac{I_t}{I_0}, \tag{1.25}$$

where I_r is the intensity of the reflected field and I_t is the intensity of the transmitted field. As we established in Eq. 1.19,

$$|\vec{p}_{ray}| \propto \Phi_{ray} \propto I.$$

As such, R & T are also the ratio of $|\vec{p}_r|$ or $|\vec{p}_t|$ and $|\vec{p}_i|$, respectively:

$$R = \frac{|\vec{p}_r|}{|\vec{p}_i|}$$

$$T = \frac{|\vec{p}_t|}{|\vec{p}_i|}.$$

The Fresnel Equations [4] establish R & T as functions of θ_i, θ_t, n_1, and n_2 by

$$R_\perp = \left(\frac{n_1 \cos\theta_i - n_2 \cos\theta_t}{n_1 \cos\theta_i + n_2 \cos\theta_t} \right)^2 \tag{1.26}$$

$$R_\parallel = \left(\frac{n_1 \cos\theta_t - n_2 \cos\theta_i}{n_1 \cos\theta_t + n_2 \cos\theta_i} \right)^2 \tag{1.27}$$

$$T_\perp = 1 - R_\perp \tag{1.28}$$

where $R_\perp$ is the reflectance if the electric field is polarized orthogonally to the plane of incidence (the plane spanned by the incident ray and normal vector) and $R_\parallel$ is the intensity coefficient if the light is polarized parallel to the plane of incidence. For the rest of this thesis, we will assume that the light is polarized so that $R_\perp$ will be the correct coefficient. This will significantly simply our later computations, but the reader should keep this assumption in mind. If we also assume that the Minkowski interpretation (Eq. 1.15) is the correct momentum to apply to our system, Eq. 1.22 is now

$$\vec{p}_{mechanical} = n_1|\vec{p}_i|\begin{pmatrix} -\cos\theta_i \\ -\sin\theta_i \end{pmatrix} - n_1 R_\perp |\vec{p}_i|\begin{pmatrix} \cos\theta_r \\ -\sin\theta_r \end{pmatrix} - n_2(1-R_\perp)|\vec{p}_i|\begin{pmatrix} -\cos\theta_t \\ -\sin\theta_t \end{pmatrix},$$

which simplifies to

$$\vec{p}_{mechanical} = |\vec{p}_i|\begin{pmatrix} -n_1\cos\theta_i - n_1 R_\perp \cos\theta_i + n_2(1-R_s)\cos\theta_t \\ -n_1\sin\theta_i + n_1 R_\perp \sin\theta_i + n_2(1-R_\perp)\sin\theta_t \end{pmatrix}.$$

Substitution of Eq. 1.21 (Snell's law) yields

$$\vec{p}_{mechanical} = |\vec{p}_i|\begin{pmatrix} -n_1(1+R_\perp)\cos\theta_i + n_2(1-R_\perp)\cos\theta_t \\ 0 \end{pmatrix}. \tag{1.29}$$

Remarkably, we discover that the change in momentum at the surface only has a component in the direction of the normal! This makes computation much easier since we can easily determine the normal of a surface at a given point. Having a tangential component would double the number of steps necessary to determine the force after a ray interacts with a body. However, we can't celebrate yet. So far, we have only applied the Minkowski momentum to Eq. 1.22, but what if the Abraham momentum is the correct momentum to apply to our system? Well, it actually doesn't matter

which momentum interpretation we use [9, 10]. Sadly, I can't rigorously prove this as it requires a relativistically-compatible, thorough electrodynamic interpretation [11][1]. The only necessary detail to include is that our ray tracing algorithm will converge to the same value regardless of the interpretation [10].

Substituting Eq. 1.19 into Eq. 1.29,

$$d\vec{p}_{mechanical} = \frac{\Phi_{ray}}{c} dt \begin{pmatrix} -n_1(1+R_\perp)\cos\theta_i + n_2(1-R_\perp)\cos\theta_t \\ 0 \end{pmatrix},$$

where Φ_{ray} is the power of the incident ray, and with some rearranging and using Newton's second law ($\vec{F} = \frac{d\vec{p}}{dt}$), we find

$$\vec{F}_{mechanical} = \frac{\Phi_{ray}}{c} \begin{pmatrix} -n_1(1+R_\perp)\cos\theta_i + n_2(1-R_\perp)\cos\theta_t \\ 0 \end{pmatrix}. \tag{1.30}$$

Eq. 1.30 will form the basis for all of our following work.

[1] Readers are encouraged to read these references for an advanced discussion of momentum in electrodynamics.

Chapter 2

Modeling Optical Wings

Now that we have a basic theory and mechanism behind radiation pressure, we can show that some bodies can experience optical lift. We will adopt the Minkowski momentum, Eq 1.15, for the rest of this thesis. From Eq 1.30, we know that every time a ray interacts with a surface, there is no momentum from the light that is transfered tangentially to the surface. This will simplify later calculations.

The force on an airfoil, $\vec{F}_{airfoil}$, is given by the Kutta-Joukowski theorem, which states

$$\vec{F}_{airfoil} = -\oint_{\nu} P_{air} \hat{da}. \tag{2.1}$$

P_{air} is the air pressure at surface element $\hat{da}$ and ν defines the surface of the airfoil [12]. Analogously, the force on a lightfoil, $\vec{F}_{lightfoil}$ is Eq. 2.1 with the radiation pressure P_{rad} substituted for P_{air}. Thus Eq. 2.1 becomes

$$\vec{F}_{lightfoil} = -\oint_{\nu} P_{rad} \hat{da}. \tag{2.2}$$

Eq. 2.2 can be applied to any arbitrary body, but can be analytically solved only for selective test cases. In order to derive the characteristic forces and torques on an arbitrary body, we need to develop a numeric procedure. In the paper *Stable Optical*

Lift, Swartzlander used the open-source optical ray tracing software POV-Ray to determine the optical forces on semicylindrical bodies [6]. We will design our own ray tracing procedure to determine these optical forces ourselves.

Consider Fig 1.4. We determined that the momentum transferred to the body is given by Eq. 1.30, which we can write as

$$\vec{F}_{ray} = \frac{\Phi_{ray}}{c}(-n_1(1+R_\perp)\cos\theta_i + n_2(1-R_\perp)\cos\theta_t)\hat{n}, \tag{2.3}$$

where $\hat{n}$ is the unit normal of the surface pointing toward the medium that the incident ray travels through. If we initialize and propagate N rays, then the net force on the body can be obtained by summing over all of the rays,

$$\vec{F}_{net} = \sum_j^N \vec{F}_{ray,j}. \tag{2.4}$$

In order to find the net torque, we need to define a center of mass for our body and a vector, $\vec{\mathcal{R}}_j$, that points from the center of mass to the position where the jth ray hits the surface of the body. The net torque on the body is then

$$\vec{\tau}_{net} = \sum_j (\vec{\mathcal{R}}_j \times \vec{F}_{ray,j}). \tag{2.5}$$

In the abstract, we defined the goal of determining a refractive body's "stable angles of attack and lift forces". What we mean by this is that, for a given body, we'll attempt to find angles of rotation, ω, about the body's center of mass where $\vec{\tau}_{net}(\omega) = 0$ and $\frac{d\vec{\tau}_{net}}{d\omega} < 0$. If both conditions are satisfied, then the body will rotate to ω and stay in that configuration if it's sufficiently damped. This isn't totally sufficient however. We also want $\vec{F}_{net}$ to have a nonzero component in the direction orthogonal to the initial propagation of the light so that we omit any trivial solutions of ω that result from symmetry. We term any angle ω that satisfies all three conditions as a "stable

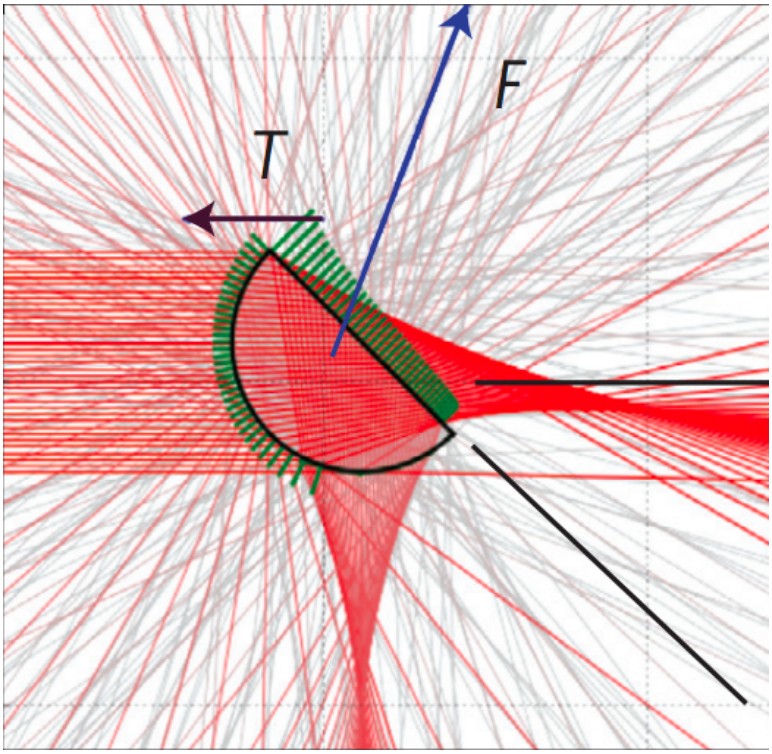

Figure 2.1: A figure from Swartzlander's paper *Stable Optical Lift* that shows the net force and torque on a semicylindrical object with rays coming from the left [6].

angle of attack".

Eqs. 2.3-2.5 form the basis for a numeric procedure based on optical ray tracing. The following section will be devoted to describing a ray tracing algorithm to find the optical forces on semicylinders.

2.1 Ray Tracing Procedure

A basic ray tracing algorithm will require the following steps:

1. Define the surface of a dielectric and initiate rays.
2. Find the intersection of the rays with the surface.
3. Determine the change in direction of the rays due to reflection and refraction.
4. Repeat steps 1 & 2 until the rays exit the surface [13].

These steps define the most basic methodology for finding the propagation of rays through a material. However, just implementing these steps will not fully solve the problem we have outlined earlier. We need to apply some additional steps to find the optical forces on the body:

- Define our rays to have some power, Φ_{ray}, flowing down their length (this is the proxy for optical momentum).
- Determine the power of reflected and transmitted rays based on the reflectance and transmittance.

All of these points must be covered in order for our ray tracing module to successfully determine the optical forces on a refractive body.

2.1.1 Defining Rays and Surfaces

In the module, a ray is an object with five parameters:

1. The number of times a ray has interacted with the body (N_{int}).
2. The ray's starting position relative to the origin ($\vec{r}_{ray} = [x_0, y_0]$).
3. The ray's direction vector ($\vec{k} = [\cos\phi, \sin\phi]$).
4. The power of the ray (Φ_{ray}).
5. A boolean that shows whether the ray is inside or outside of the body (B).

Here, ϕ is the angle between the ray's propagation direction and the horizontal, and $B = True$ implies that the ray is inside of the body. The boolean is important because it allows us to determine the ray's incident and transmission medium rather easily.

The surface of a dielectric is defined by the root of a function, $F(x, y)$, so that the set of points in (x, y) where

$$F(x, y) = 0 \tag{2.6}$$

defines the surface. Some surface function examples are given below.

Surface	$F(x, y)$
Circle (radius R)	$x^2 + y^2 - R^2$
Vertical Plane	x
Horizontal Plane	y

In addition to defining the surface of our dielectric body, we also define its index of refraction $n_{material}$. For simplicity, we'll assume that the medium on the exterior of the body is just a vacuum. By definition, the index of refraction of a vacuum is $n_{vacuum} = 1$.

2.1.2 Finding Ray Intersections

The parametric equation of a single ray is given by

$$Q(s) = \begin{pmatrix} x_0 + ls \\ y_0 + ms \end{pmatrix} \quad s \in [0, a] \tag{2.7}$$

where s is the parameter of distance and a is the constant such that when $s = a$, the ray intersects the surface of the dielectric. To continue, we have to find a for an arbitrary $F(x, y)$. If we substitute Eq. 2.7 into Eq. 2.6, then

$$F(Q(s)) = 0. \tag{2.8}$$

We then need to find the value $s = a$ that satisfies Eq. 2.8. However, in many cases, the solution to Eq. 2.8 will be transcendental and, thus, not analytically solvable to

arbitrary precision. To get around this problem, we introduce the Newton-Raphson method of root finding.

Newton-Raphson

Let some function P(x) have a root at x_{root}. Given some guess as to the location of the root, x_{guess}, we can ask how far away x_{guess} is away from the root. In other words, if $\delta = x_{root} - x_{guess}$, then what is δ? If we Taylor expand P(x) around x_{root}, we attain

$$P(x_{root}) = P(x_{guess} + \delta) \approx P(x_{guess}) + \delta P'(x_{guess}) + \cdots.$$

And, by assumption,

$$0 = P(x_{guess}) + \delta P'(x_{guess}) + \cdots$$

The linear approximation to δ that solves this equation is

$$\delta_{linear} = -\frac{P(x_{guess})}{P'(x_{guess})}.$$

Now let $x_1 = x_{guess}$. Using δ_{linear}, we can also update our guess so that it's closer to x_{root}. Let's define our new guess, x_2, as

$$x_2 = x_1 - \frac{P(x_1)}{P'(x_1)}. \tag{2.9}$$

If we feel that x_2 isn't close enough to the function's root, then we can update our guess to x_3 where

$$x_3 = x_2 - \frac{P(x_2)}{P'(x_2)}.$$

Following this pattern, we keep defining a new guess until we reach x_j. We define a quantity ϵ such that x_j satisfies $|P(x_j)| < \epsilon$, which determines when we stop iterating. [14].

2.1.3 Determining $\hat{n}$

Using Newton-Raphson, we can now solve for a in Eq. 2.8 for any surface. The next step requires us to find the normal vector, $\hat{n}$, where the ray intersects the surface. Since we now have a, we can solve for the point in the x-y plane that the ray intersects with the surface. We define this point as $Q(a) = \begin{pmatrix} x_0 + l\ a \\ y_0 + m\ a \end{pmatrix}$. The normal of the surface at this point is

$$\hat{n} = \frac{1}{\sqrt{\left(\frac{dF}{dx}(Q(a))\right)^2 + \left(\frac{dF}{dy}(Q(a))\right)^2}} \begin{pmatrix} \frac{dF}{dx}(Q(a)) \\ \frac{dF}{dy}(Q(a)) \end{pmatrix}. \tag{2.10}$$

Whether $\hat{n}$ points out of a closed surface or into a closed surface depends on how one defines $F(x, y)$. Either way, we want $\hat{n}$ to point from the surface into the medium of index n_1 (i.e. the medium containing the incident ray), which Eq. 2.10 won't satisfy for every ray. We create a condition

$$\text{If}$$
$$-\vec{\mathbf{I}} \cdot \hat{n} < 0,$$
$$\text{Then}$$
$$\hat{n} = -\hat{n}$$

that assures $\hat{n}$ is pointing in the correct direction, where $\vec{\mathbf{I}}$ is the normalized direction vector of the incident ray.

Now that we have the point of intersection and the unit normal at that intersection, we can change the direction of our rays due to reflection and transmission.

2.1.4 Reflection

Using Eq. 1.20 (law of reflection), we know that the angle between the incident ray and the normal is the same as the angle between the reflected ray and normal. One

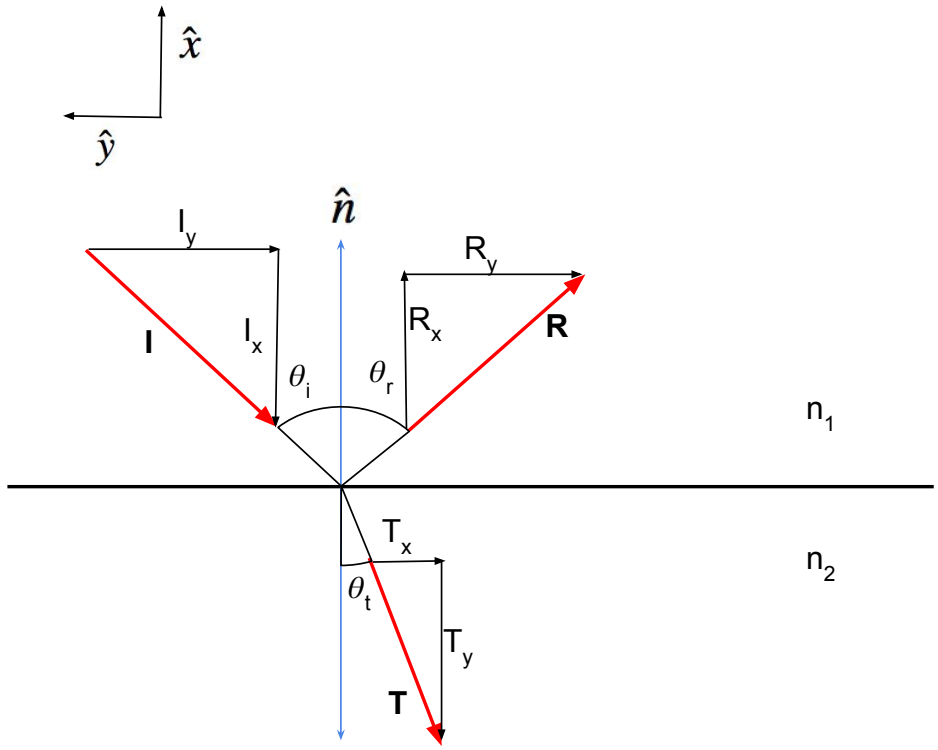

Figure 2.2: The incident, reflected and transmitted rays and their normal and tangential components are depicted. Using the law of reflection and Snell's law, we attempt to describe the direction of $\vec{\mathbf{R}}$ and $\vec{\mathbf{T}}$ using only $\vec{\mathbf{I}}$.

could find θ_i and use that to determine the new direction of the ray at an angle relative to the surface, but this would require a multiple rotations of the original reference frame to convert this direction into the original reference coordinates. Instead, we can use the vector form of the law of reflection to solve for the reflected ray direction more efficiently [15].

Law of Reflection (vector form)

Let $\vec{\mathbf{I}}$ be the normalized direction vector of the incident ray. As shown in Fig. 2.2, we can separate $\vec{\mathbf{I}}$ into components that are normal to and tangential to the surface, $\mathbf{I}_x$ and $\mathbf{I}_y$. Similarly, we can separate the normalized direction vector for the reflected

ray $\vec{\mathbf{R}}$ into normal and tangential components $\mathbf{R}_x$ and $\mathbf{R}_y$. One can see from Fig 2.2 that

$$|\mathbf{R}_x| = \cos\theta_r$$

and

$$|\mathbf{I}_x| = \cos\theta_i.$$

As a consequence of the law of reflection,

$$|\mathbf{R}_x| = \cos\theta_r = \cos\theta_i = |\mathbf{I}_x|$$

and from the definition of the dot product,

$$|\mathbf{I}_x| = |\mathbf{R}_x| = (-\vec{\mathbf{I}} \cdot \hat{n}).$$

However, since $\mathbf{I}_x < 0$ (i.e. the ray is headed toward the surface) and $\vec{\mathbf{R}}_x > 0$, we obtain the relation

$$\mathbf{R}_x\hat{n} = -\mathbf{I}_x\hat{n} = (-\vec{\mathbf{I}} \cdot \hat{n})\hat{n}. \tag{2.11}$$

Using the same steps as above and the knowledge that $|\mathbf{R}_y| = \sin\theta_r$, we can also see that

$$\mathbf{R}_y\hat{y} = \mathbf{I}_y\hat{y} = \vec{\mathbf{I}} - \mathbf{I}_x\hat{n}. \tag{2.12}$$

we can substitute Eqs. 2.11 & 2.12 into $\vec{\mathbf{R}} = \mathbf{R}_x\hat{n} + \mathbf{R}_y\hat{y}$ and obtain

$$\vec{\mathbf{R}} = (\vec{\mathbf{I}} - (\vec{\mathbf{I}} \cdot \hat{n})\hat{n}) - (\vec{\mathbf{I}} \cdot \hat{n})\hat{n}$$

$$\vec{\mathbf{R}} = \vec{\mathbf{I}} - 2\ (\vec{\mathbf{I}} \cdot \hat{n})\hat{n} \tag{2.13}$$

Using Eq. 2.13, we can now determine the direction of the reflected ray's direction of propagation for any $\hat{n}$ and $\vec{\mathbf{I}}$ without any superfluous steps [15].

2.1.5 Transmission

Similar to reflection, we require a vector form of Snell's law. This will significantly reduce the computational complexity of our algorithm.

Snell's Law (vector form)

Let $\vec{\mathbf{T}}$ be the normalized direction vector of the transmitted ray. We can separate $\vec{\mathbf{T}}$ in components normal to and tangential to the surface, $\mathbf{T}_x$ and $\mathbf{T}_y$, respectively. From Eq. 1.21, we know that

$$\sin\theta_t = \frac{n_1}{n_2}\sin\theta_i,$$

which is equivalent to

$$\mathbf{T}_y = \frac{n_1}{n_2}\,\mathbf{I}_y. \tag{2.14}$$

At this point, one can see that there is a problem if $\sin\theta_i > \frac{n_2}{n_1}$. If that is the case, then $\sin\theta_t$ would be greater than 1, which isn't possible. This leaves us with a caveat that the rest of this derivation requires the condition $\sin\theta_i \leq \frac{n_2}{n_1}$ (we will deal with the other case later).

Since $\vec{\mathbf{I}} = \mathbf{I}_x\hat{n} + \mathbf{I}_y\hat{y}$, we can rewrite Eq. 2.14 as

$$\mathbf{T}_y\hat{y} = \frac{n_1}{n_2}\,(\vec{\mathbf{I}} - \mathbf{I}_x\hat{n}) = \frac{n_1}{n_2}\,(\vec{\mathbf{I}} - (\vec{\mathbf{I}}\cdot\hat{n})\,\hat{n}). \tag{2.15}$$

The Pythagorean theorem tells us

$$|\vec{\mathbf{T}}|^2 = |\mathbf{T}_x|^2 + |\mathbf{T}_y|^2,$$

Since $|\vec{\mathbf{T}}| = 1$, the Pythagorean theorem simplifies to

$$|\mathbf{T}_x|\hat{n} = -\sqrt{1 - |\mathbf{T}_y|^2}\;\hat{n}. \tag{2.16}$$

Now, we can obtain $\vec{\mathbf{T}}$ by the sum of $\mathbf{T}_x\hat{n}$ and $\mathbf{T}_y\hat{y}$:

$$\vec{\mathbf{T}} = \frac{n_1}{n_2}\,(\vec{\mathbf{I}} - (\vec{\mathbf{I}}\cdot\hat{n})\,\hat{n}) - \sqrt{1-|\mathbf{T}_y|^2}\,\hat{n}$$

$$\vec{\mathbf{T}} = \frac{n_1}{n_2}\,\vec{\mathbf{I}} + \left(\frac{n_1}{n_2}(-\vec{\mathbf{I}}\cdot\hat{n}) - \sqrt{1-|\mathbf{T}_y|^2}\right)\,\hat{n}.$$

We also know that the magnitude of the tangential component, $|\mathbf{T}_y|$, is $\sin\theta_t$ and, by the definition of the dot product, $-\vec{\mathbf{I}}\cdot\hat{n} = \cos\theta_i$. With that in mind, the transmission direction vector is

$$\vec{\mathbf{T}} = \frac{n_1}{n_2}\vec{\mathbf{I}} + \left(\frac{n_1}{n_2}(-\vec{\mathbf{I}}\cdot\hat{n}) - \sqrt{1-(\sin\theta_t)^2}\right)\,\hat{n},$$

which is equivalent to

$$\vec{\mathbf{T}} = \frac{n_1}{n_2}\vec{\mathbf{I}} + \left(\frac{n_1}{n_2}(-\vec{\mathbf{I}}\cdot\hat{n}) - \sqrt{1-\left(\frac{n_1}{n_2}\sin\theta_i\right)^2}\right)\,\hat{n}$$

or

$$\vec{\mathbf{T}} = \frac{n_1}{n_2}\vec{\mathbf{I}} + \left(\frac{n_1}{n_2}(-\vec{\mathbf{I}}\cdot\hat{n}) - \sqrt{1-\left(\left(\frac{n_1}{n_2}\right)^2(1-\cos\theta_i{}^2)\right)}\right)\,\hat{n}.$$

Finally, we can totally express $\vec{\mathbf{T}}$ with vector operations with

$$\vec{\mathbf{T}} = \frac{n_1}{n_2}\vec{\mathbf{I}} + \left(\frac{n_1}{n_2}(-\vec{\mathbf{I}}\cdot\hat{n}) - \sqrt{1-\left(\left(\frac{n_1}{n_2}\right)^2\left(1-\left(-\vec{\mathbf{I}}\cdot\hat{n}\right)^2\right)\right)}\right)\,\hat{n}. \tag{2.17}$$

Total Internal Reflection

We're not quite done with transmission yet. For the case of $\sin\theta_i \geq \frac{n_2}{n_1}$, Eq. 2.17 is unusable. We define an angle of incidence, θ_c, such that $\theta_t = \frac{\pi}{2}$. From Eq. 1.21,

$$\sin\theta_c = \frac{n_2}{n_1}\sin\frac{\pi}{2} = \frac{n_2}{n_1}.$$

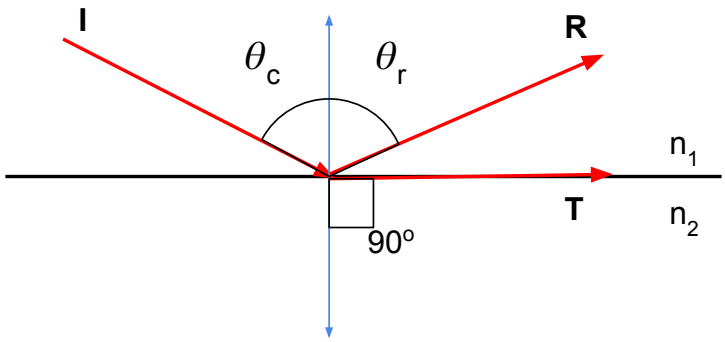

Figure 2.3: An incident ray intersects the interface at θ_c. At this angle, the transmitted ray is orthogonal to $\hat{n}$ and all of the incoming energy is reflected. This can only occur if $n_1 > n_2$.

Thus,

$$\theta_c = \arcsin \frac{n_2}{n_1}.$$

If a ray interacts with a dielectric interface at an angle of incidence, θ_i, greater or equal to θ_c, then all of the incoming radiant energy is reflected back into the material [4]. This condition is known as total internal reflection. We account for this condition in our ray tracing procedure by neglecting to generate a transmitted ray and set the power of the reflected ray equal to the power of the incident ray.

New Rays

Using Eqs. 2.13 & 2.17, we can now generate the reflected and transmitted ray based upon $\hat{n}$ and $\vec{\mathbf{I}}$. Both new rays will have position $\vec{r}_{ray} = Q(a)$ (the point where the incident ray contacts the body) and the new ray directions $\vec{k}_r = \vec{\mathbf{R}}$ and $\vec{k}_t = \vec{\mathbf{T}}$, where $\vec{k}_r$ is the reflected ray direction and $\vec{k}_t$ is the transmitted ray direction. To find the radiant power of the new rays, we look back to Eqs. 1.26 & 1.28. If $\Phi_{incident}$ is the

power of the incident ray, then

$$\Phi_{reflect} = R_{\perp}\ \Phi_{incident} \tag{2.18}$$

and

$$\Phi_{Transmitted} = T_{\perp}\ \Phi_{incident}, \tag{2.19}$$

where $\Phi_{reflect}$ and $\Phi_{transmitted}$ is the power of the reflected and transmitted ray, respectively. In addition, we need to update our interaction number. If the incident ray has interacted with the body $N_{int,i}$ times, then the interaction count for the reflected and refracted ray, $N_{int,r}$ & $N_{int,t}$, is

$$N_{int,r} = N_{int,t} = N_{int,i} + 1.$$

This parameter is important because it allows us to specify how many times we want the rays to bounce around inside of the body. In theory, these rays can continuously be reflected off of the inside of the surface and never escape, but the power of the rays inside of the surface will rapidly converge to zero as N_{int} increases. We'll typically set an upper bound for N_{int} at three or four since the power of the rays at $N_{int} = 3$ is $\approx 1\%$ of its power before it ever interacts with the surface.

If the incident ray experiences total internal reflection, the procedure outlined above isn't sufficient. In this case, there is no transmitted ray and all of the incoming energy from the incident ray will be reflected back into the surface [4]. Our procedure accounts for this by simply neglecting to generate a transmitted ray and setting

$$\Phi_{reflected} = \Phi_{incident}$$

and

$$\vec{k}_r = \vec{\mathbf{R}}.$$

We're only missing a change in one ray parameter now. If the incident ray originates outside of the surface, then its boolean, $B_{incident} = False$. Consider the case where this incident ray interacts with the body without total internal reflection, then a reflected and transmitted ray will be produced. It's quite trivial to determine $B_{reflected}$ and $B_{transmitted}$ since we know that the reflected ray will propagate back into the medium that the incident ray originated from. With that knowledge, we know that

$$B_{reflected} = B_{incident}.$$

By definition, the transmitted ray propagates into the body that the incident ray interacted with. Thus,

$$B_{transmitted} = \neg B_{incident}.$$

But, why do we care about B? The indices of refraction in Eq. 2.17, n_1 & n_2, represent the index of refraction of the medium that the incident ray travels through and the medium that the transmitted ray propagates into, respectively. Note that n_1 and n_2 aren't the same for every ray. For a ray that propagates through the interior of the body ($B = True$):

$$n_1 = n_{material}$$

and

$$n_2 = n_{vacuum} = 1.$$

Similarly, if $B = False$, then

$$n_1 = n_{vacuum} = 1$$

and

$$n_2 = n_{material}.$$

In addition, if $B = False$ and $N_{int} \neq 0$, then we can stop tracking the ray since it

will simply propagate to spatial infinity.

With all of this, we've designed a pretty competent ray tracing algorithm. Sadly, we can't celebrate yet; the optical forces on this body are yet to be determined.

2.1.6 Optical Forces

From Eq. 2.3, we have that the force that a ray of light exerts on a body is

$$F_{ray} = \frac{\Phi_{ray}}{c}(-n_1(1+R_\perp)\cos\theta_i + n_2(1-R_\perp)\cos\theta_t)\hat{n}. \tag{2.20}$$

Every time a ray interacts with the surface of a body, a force, F_{ray} is exerted on the body at the position that the ray intersects the body. More formally, a ray generates a force at position $Q(a)$, and, combining Eq. 2.20 & 2.10, Eq. 2.20 becomes

$$F_{ray} = \pm\frac{\Phi_{ray}}{c}\frac{(-n_1(1+R_\perp)\cos\theta_i + n_2(1-R_\perp)\cos\theta_t)}{\sqrt{\left(\frac{dF}{dx}(Q(a))\right)^2 + \left(\frac{dF}{dy}(Q(a))\right)^2}}\begin{pmatrix}\frac{dF}{dx}(Q(a))\\ \frac{dF}{dy}(Q(a))\end{pmatrix}$$

in cartesian coordinates. It is important to note that we now have all of the values necessary to calculate F_{ray} using the procedure outlined in this chapter. Using Eqs. 2.4 & 2.5, we have determined the net force and torque on the body using optical ray tracing. To test the accuracy of this procedure, we will solve for the torque in an analytically solvable system and then apply the procedure we have described in this chapter.

2.2 Reflective Semicylinder

Consider a semicylinder that reflects all incident radiation and doesn't allow for any transmission. Our goal is to find the torque on this body if we have a monochromatic plane wave coming from the right. Thankfully, the plane wave will simply reflect off

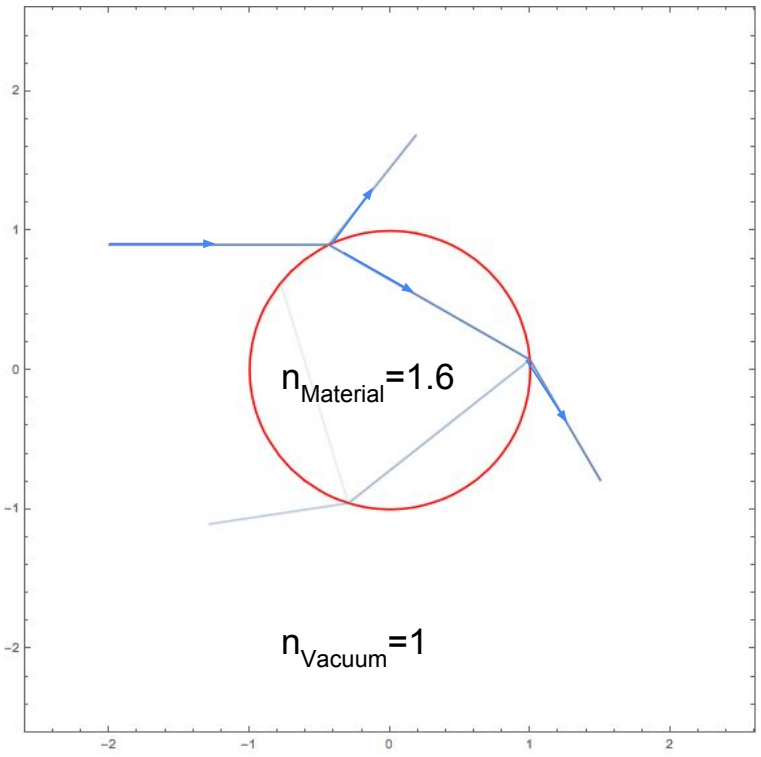

Figure 2.4: The visual output of the *Mathematica* module. A sphere of $radius = 1$ and index of refraction $n_{material} = 1.6$ is illuminated by a single ray propagating to the right from $\vec{r}_{ray} = \begin{pmatrix} -2 \\ .9 \end{pmatrix}$. Note that the rays that remain in the body rapidly lose energy as they interact with the surface of the body.

of this body and never interact with it again; allowing us to solve for the net torque using Eqs. 1.10 & 2.2. The system in an unrotated configuration is depicted in Fig 2.5. After solving for the torque in this system, we will solve for the torque of this semicylinder rotated an angle ω counterclockwise. Let the plane wave have intensity I and travel in the $-\hat{x}$ direction. From Eq. 1.10 the reflective radiation pressure on the body is

$$P_{rad} = 2\,\frac{I}{c}\cos^2\alpha,$$

and, from Eq. 2.2, the net force on the body is

$$\vec{F}_{lightfoil} = -\int_{\nu} P_{rad}\;\vec{da}.$$

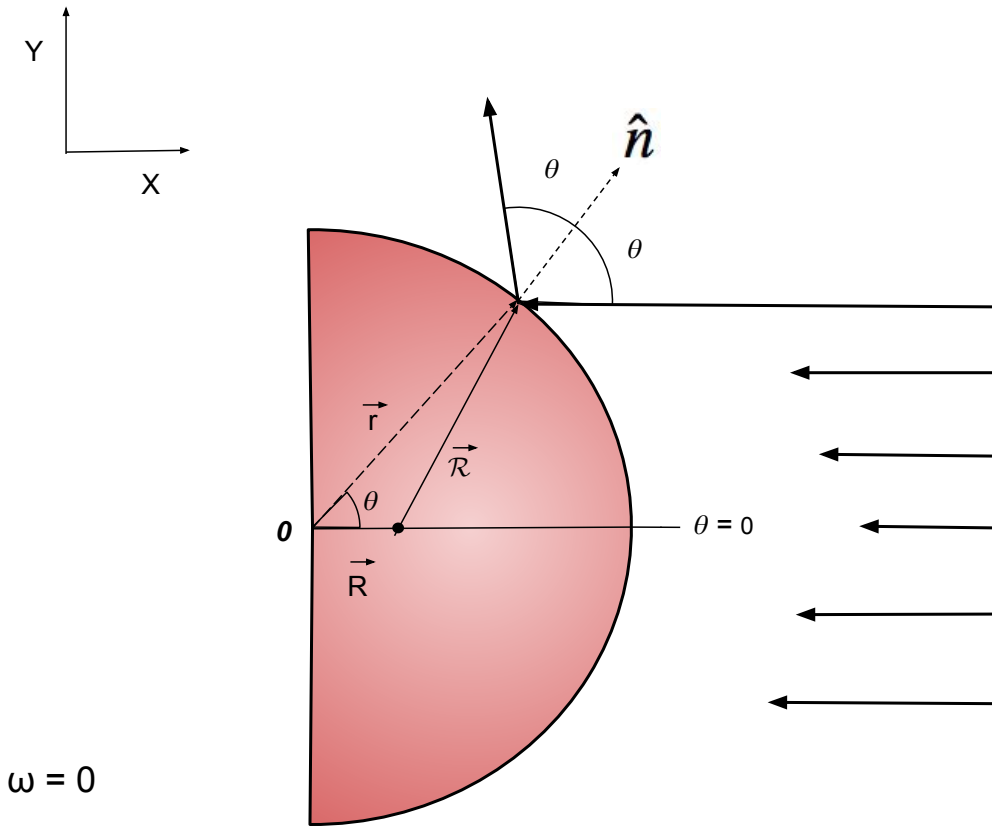

Figure 2.5: An unrotated semicylinder reflects all of the incident radiation. The vectors relevant to integration are $\vec{R}$, the position of the center of mass relative to the origin $\boldsymbol{0}$, $\vec{r}$, the position of a point relative to the origin, and $\vec{\mathcal{R}}$, the position of a point relative to the center of mass.

Combining these equations and, since $\hat{da}$ points in the $\hat{n}$ direction, Eq. 2.2 becomes

$$\vec{F}_{lightfoil} = -2\,\frac{I}{c}\int_{\nu}\cos^2\alpha\;\hat{n}\;da,$$

where da is now an infinitesimal scalar area element. Continuing requires us to define integration bounds. ν is simply half of a circle, and α, the angle between the plane wave and the normal of the surface, is equivalent to θ, the polar angle that defines a

point on the surface. The force on the lightfoil becomes

$$\vec{F}_{lightfoil} = -2\,\frac{I}{c}\int_{-\pi/2}^{\pi/2} \hat{n}\ \cos^2\theta\ d\theta.$$

For any point on a circle, $\hat{n} = \begin{pmatrix}\cos\theta\\ \sin\theta\end{pmatrix}$ so we can further simplify Eq. 2.2 to

$$\vec{F}_{lightfoil} = -2\,\frac{I}{c}\int_{-\pi/2}^{\pi/2} \begin{pmatrix}\cos\theta\\ \sin\theta\end{pmatrix}\ \cos^2\theta\ d\theta = -\frac{8I}{3c}\ \hat{x}. \tag{2.21}$$

We're close, but Eq 2.2 won't deliver the net torque on the body. Let $\vec{R}$ be the vector pointing from the center of the circle (i.e. the origin) to the center of mass and $\vec{r}$ be the vector pointing from the center of the circle to an arbitrary point on the surface of the semicylinder (see Fig. 2.5). Since the center of the circle is chosen to be at the origin and we know the center of mass of a half circle,[1]

$$\vec{R} = \begin{pmatrix}\frac{4}{3\pi}\\ 0\end{pmatrix}. \tag{2.22}$$

Define a vector $\vec{\mathcal{R}}$ that points from the center of mass of the semicylinder to the point designated by $\vec{r} = \begin{pmatrix}\cos\theta\\ \sin\theta\end{pmatrix}$. From Fig 2.5, one can see that

$$\vec{\mathcal{R}} = \vec{r} - \vec{R} = \begin{pmatrix}\cos\theta - \frac{4}{3\pi}\\ \sin\theta\end{pmatrix}. \tag{2.23}$$

[1]Curious readers can see the appendix for a derivation of the center of mass of a semicylinder.

The torque on this body is thus

$$\vec{\tau}_{net} = \int_{\nu} d\vec{\tau} = \int_{-\pi/2}^{\pi/2} \left(\vec{\mathcal{R}} \times d\vec{F} \right), \tag{2.24}$$

Since $\vec{\mathcal{R}}$ and $\vec{F}$ lie in the x-y plane, $\vec{\tau}_{net}$ only has a component in the $\hat{z}$ direction (out of the page) and Eq. 2.24 simplifies to

$$\vec{\tau}_{net} = \left(\int_{-\pi/2}^{\pi/2} \frac{8\ I\ \cos^2\theta\ \sin\theta}{3\ \pi\ c}\ d\theta \right)\ \hat{z}. \tag{2.25}$$

After calculating the integral, Eq 2.25 becomes

$$\vec{\tau}_{net} = 0.$$

Now consider the system in Fig 2.6. The semicylinder is rotated an angle ω counter-clockwise with respect to the system depicted in Fig 2.5. In order to solve for the torque of this body, we need to separate our solution into two cases. If $|\omega| \leq \frac{\pi}{2}$, the light will only illuminate the curved portion of the body. However, if $|\omega| > \frac{\pi}{2}$, then the flat portion of the semicylinder will be illuminated, complicating our calculations. Let us deal with the $|\omega| \leq \frac{\pi}{2}$ case first.

For $|\omega| \leq \frac{\pi}{2}$, the torque has a similar form to Eq. 2.25. We found the center of mass, $\vec{R}$, in the unrotated case above. Define $\vec{R}_{initial}$ to be Eq. 2.22. The center of mass in the rotated system is

$$\vec{R} = \mathbf{\Omega}(\omega)\ \vec{R}_{initial}, \tag{2.26}$$

where $\mathbf{\Omega}(\omega)$ is the two dimensional rotation matrix,

$$\mathbf{\Omega}(\omega) = \begin{pmatrix} \cos\omega & -\sin\omega \\ \sin\omega & \cos\omega \end{pmatrix}. \tag{2.27}$$

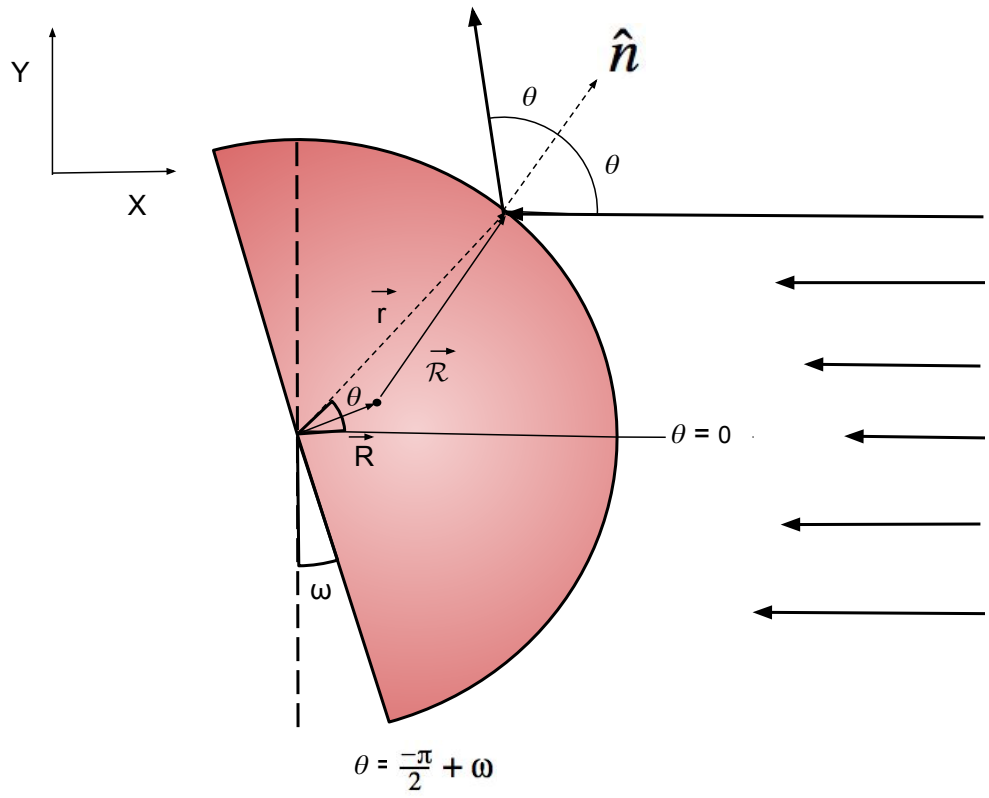

Figure 2.6: The semicylinder is rotated an angle ω from the horizontal. The vectors relevant to integration and the value of θ for the lower integration bound are shown.

Combining Eqs. 2.26 & 2.27, the center of mass of the system becomes

$$\vec{R} = \begin{pmatrix} \cos\omega & -\sin\omega \\ \sin\omega & \cos\omega \end{pmatrix} \begin{pmatrix} \frac{4}{3\ \pi} \\ 0 \end{pmatrix} = \begin{pmatrix} \frac{4}{3\ \pi}\cos\omega \\ \frac{4}{3\ \pi}\sin\omega \end{pmatrix}.$$

$\vec{R}$ is the center of mass in both of the cases outlined above. As a consequence,

$$\vec{\mathcal{R}} = \begin{pmatrix} \cos\theta - \frac{4}{3\ \pi}\cos\omega \\ \sin\theta - \frac{4}{3\ \pi}\sin\omega \end{pmatrix}.$$

In addition to a new center of mass, the integration bounds change with rotation.

Looking at Fig. 2.6, the lower integration bound becomes $-\frac{\pi}{2}+\omega$ with a net counterclockwise rotation. With the new integration bounds and center of mass, the net torque on the body becomes

$$\tau_{net} = \int_{-\pi/2+\omega}^{\pi/2} \left(\vec{\mathcal{R}} \times d\vec{F}\right),$$

which simplifies to

$$\vec{\tau}_{net} = \int_{-\pi/2+\omega}^{\pi/2} \left(\frac{8\ I\ \cos^2\theta\ \sin(\theta-\omega)}{3\ \pi\ c}\right) d\theta\ \hat{z} = -\frac{16\ I\ (1+\cos\omega)\sin\omega}{9\ \pi\ c}\ \hat{z}.$$

Similarly, for a net clockwise rotation, the upper integration bound becomes $\frac{\pi}{2}+\omega$ (note that $\omega < 0$ for a net clockwise rotation and so $\frac{\pi}{2}+\omega < \frac{\pi}{2}$). In this case,

$$\vec{\tau}_{net} = \int_{-\pi/2}^{\pi/2+\omega} \left(\frac{8\ I\ \cos^2\theta\ \sin(\theta-\omega)}{3\ \pi\ c}\right) d\theta\ \hat{z} = \frac{16\ I\ (1+\cos\omega)|\sin\omega|}{9\ \pi\ c}\ \hat{z}.$$

This conforms to our expectations. The symmetry of the body implies that the magnitude of the torque for a counterclockwise rotation of ω is the same as for a clockwise rotation of ω, but opposite in direction. We still need to find the torque for the case of $|\omega| > \frac{\pi}{2}$. Consider Fig 2.7. We now have reflections off of the flat portion of our surface, and our simple integration bounds in Eq. 2.25 are no longer valid. We'll split the torque on the body into two components; one dependent on the curved and one dependent on the flat portion of the surface. The torque is thus

$$\vec{\tau}_{net} = \int_{\nu} d\tau_{curve} + \int_{\phi} d\tau_{flat},$$

where ν is the curved portion of the body and ϕ is the flat portion of the body. Let us define a parametric function $\vec{r}(t)$ that traces the flat portion of the semicylinder,

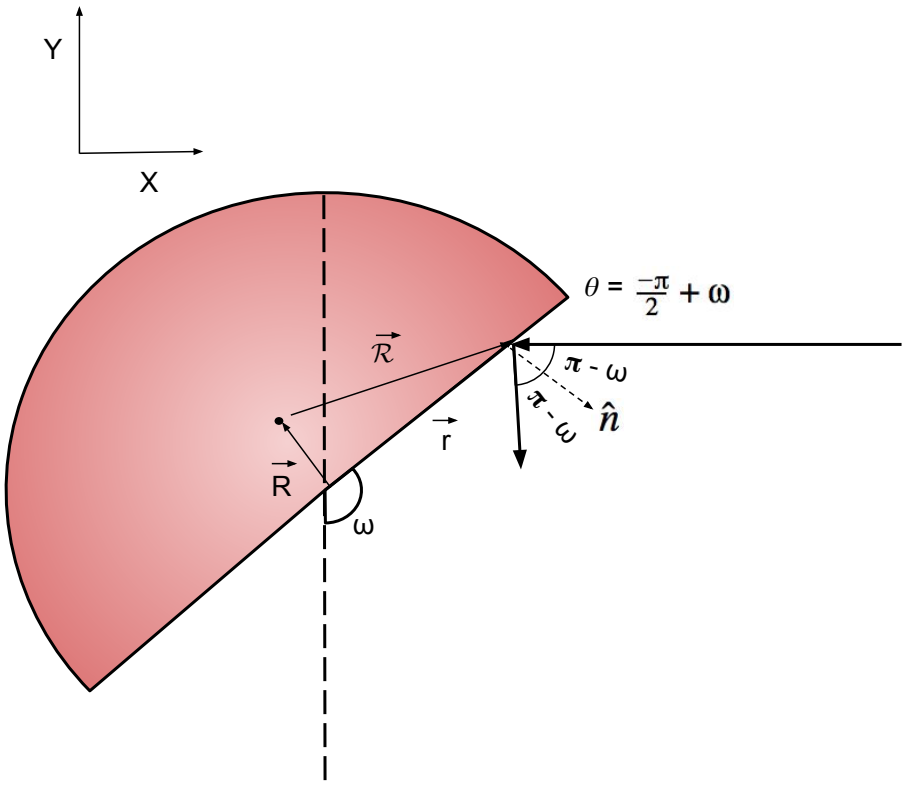

Figure 2.7: The reflective semicylinder with $\frac{\pi}{2} < \omega < \frac{3\,\pi}{2}$. The incident radiation will reflect off of the flat portion of the semicylinder at $\theta_i = \pi - \omega$.

a line at an angle ω to the vertical

$$\vec{r}(t) = \begin{pmatrix} t\sin\omega \\ -t\cos\omega \end{pmatrix} \qquad t \in [-1, 1]. \tag{2.28}$$

The length of this line is two. Focusing exclusively on the flat portion of the surface, $\vec{\mathcal{R}}(t)$ is

$$\vec{\mathcal{R}}(t) = \vec{r}(t) - \vec{R} = \begin{pmatrix} t\sin\omega - \frac{4}{3\pi}\cos\omega \\ -t\cos\omega - \frac{4}{3\pi}\sin\omega \end{pmatrix},$$

where $\frac{\pi}{2} \leq \omega \leq \frac{3\pi}{2}$. To find $\vec{F}(t)$, the force at a particular point on the flat surface,

we look to Fig. 2.7 and can see that $\hat{n} = -\begin{pmatrix}\cos\omega\\ \sin\omega\end{pmatrix}$. From Eqs. 2.2 & 1.10,

$$\vec{F}_{net} = -\int_{\phi} F(t)\hat{n}\ dt = \int_{-1}^{1}\left(\frac{2\ I}{c}\cos^2\omega\right)\ \begin{pmatrix}-\cos\omega\\ -\sin\omega\end{pmatrix} dt = -\frac{4\ I}{c}\cos^2\omega\ \hat{n} = F\ \hat{n}.$$

One can see that $\vec{F}_{net}$ is independent of t. The torque about the center of mass of the flat portion of the body becomes

$$\vec{\tau}_{flat} = \int_{-1}^{1}(\vec{\mathcal{R}}(t) \times F\hat{n}\ dt).$$

Since F is independent of t and $\vec{\mathcal{R}} \times \hat{n} = -t\ \hat{z}$,

$$\vec{\tau}_{flat} = F\int_{-1}^{1}(\vec{\mathcal{R}}(t) \times \hat{n}\ dt) = -F\int_{-1}^{1} t\ dt\ \hat{z} = 0.$$

Thus, the flat portion contributes no torque to the reflective semicylinder.

Now we find that the net torque on this body for $|\omega| > \frac{\pi}{2}$ has the same form as the $|\omega| \leq \frac{\pi}{2}$ case:

$$\vec{\tau}_{net} = \int_{\nu} d\vec{\tau}_{curve} + 0 = -\frac{16\ I\ (1+\cos\omega)\sin\omega}{9\ \pi\ c}\ \hat{z}. \tag{2.29}$$

Fig. 2.8 shows a plot of $\tau_z \cdot c$ vs. ω, where c is the speed of light and τ_z is the z-component of the torque about the center of mass, given by the above equation with $I = 1\frac{\text{Watt}}{\text{m}^2}$. Looking at Fig. 2.8 & Eq. 2.29, the torque is zero only for $\omega = 0$ and $\omega = \pi$, but we don't know whether either of these points are stable. The derivative of Eq. 2.29 with respect to ω is

$$\frac{d\tau_z}{d\omega}(\omega) = -\frac{16(\cos\omega + \cos^2\omega - \sin^2\omega)}{9\ c\ \pi}.$$

For $\omega = 0$ and $\omega = \pi$, $\frac{d\tau_z}{d\omega} = -\frac{32}{9c\ \pi}$ and $\frac{d\tau_z}{d\omega} = 0$, respectively. Recall that rotational stability only occurs for $\frac{d\tau_z}{d\omega} < 0$, so the reflective semicylinder only has a stable angle of attack at $\omega = 0$. It's clear that this stable point is as a result of the symmetry of the semicylinder at $\omega = 0$, and so we expect $\vec{F}_{net}$ to only have a component in the $\hat{x}$ direction. Eq. 2.21 shows that this is indeed true,

$$c \cdot \vec{F}_{net} = \begin{pmatrix} -\frac{8}{3} \\ 0 \end{pmatrix} \quad \left(\frac{Nm}{s}\right).$$

Now, we will apply our ray tracing procedure to see if there's any discrepancy between the numeric and analytic solution. We will use the procedure to generate and propagate 100 rays from the right. Every ray will start with an interaction number $N_{int} = 0$, an x-component of $\vec{r}_{ray} = 2$, a direction vector $\vec{k} = [-1, 0]$, and $B = False$. Since we want all of our rays to intersect the surface, the topmost ray should have a position $\vec{r}_{ray,top} = [2, 1]$ for a rotation $0 \leq \omega \leq \pi$, a $\vec{r}_{ray,top} = [-2, -\cos\omega]$ for $\pi < \omega \leq \frac{3\ \pi}{2}$, and a $\vec{r}_{ray,top} = [-2, \cos\omega]$ for $\frac{3\ \pi}{2} < \omega < 2\ \pi$. Similarly, the position of the bottommost ray that will intersect the rotated semicylinder is $\vec{r}_{ray,bottom} = [2, -\cos\omega]$ for $0 \leq \omega \leq \frac{\pi}{2}$, $\vec{r}_{ray,bottom} = [2, \cos\omega]$ for $\frac{\pi}{2} < \omega \leq \pi$, and $\vec{r}_{ray,bottom} = [2, -1]$ for $\pi < \omega < 2\ \pi$.

To find the staring position of all 100 rays, we define a distance

$$\Delta x = \frac{L}{N_{rays} - 1} = \frac{L}{99}, \tag{2.30}$$

where L is the distance between $\vec{r}_{ray,bottom}$ and $\vec{r}_{ray,top}$. Ostensibly, L can be given by four different equations for the four rotation regimes shown in Fig 2.9.

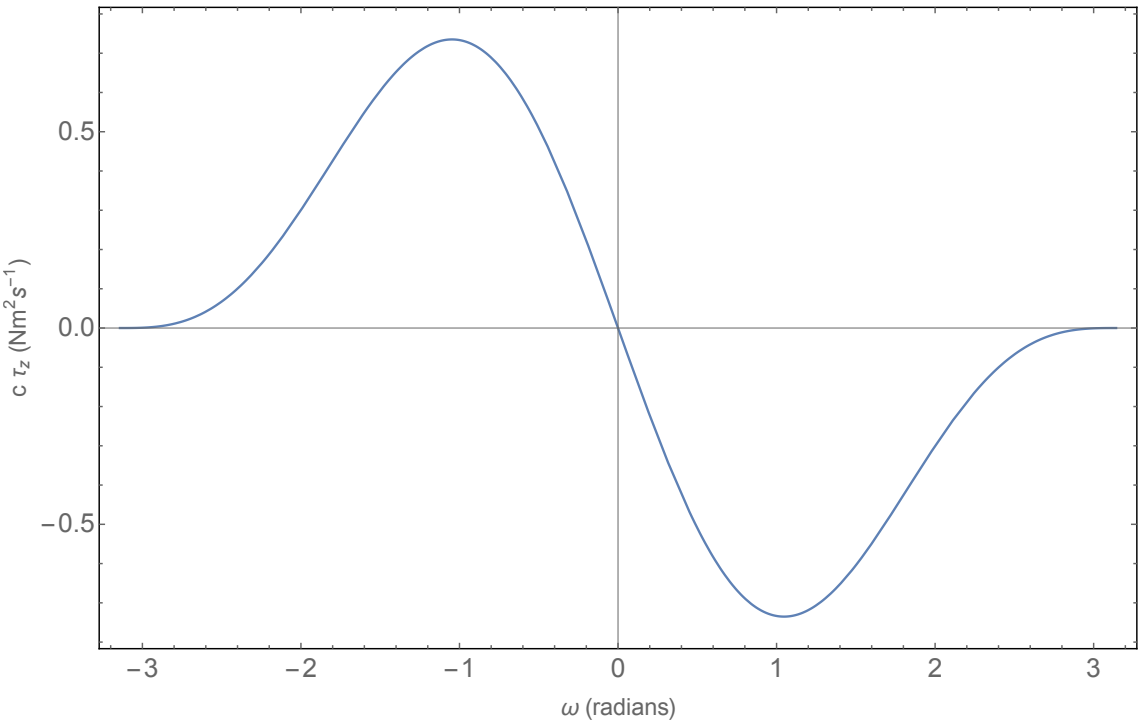

Figure 2.8: The magnitude of the torque in the $\hat{z}$ direction times c, τ_z c vs. ω for a reflective semicylinder. There's only one rotationally stable point for this surface at $\omega = 0$, which results in no lift force.

$$L(\omega) = \begin{cases} |1 + \cos\omega|, & \text{if } 0 \leq \omega \leq \dfrac{\pi}{2} \\ |1 - \cos\omega|, & \text{if } \dfrac{\pi}{2} < \omega \leq \pi \\ |-1 + \cos\omega|, & \text{if } \pi < \omega \leq \dfrac{3\pi}{2} \\ |\cos\omega + 1|, & \text{if } \dfrac{3\pi}{2} < \omega < 2\pi \end{cases}.$$

This simplifies slightly to just two cases since $|1 - \cos\omega| = |\cos\omega - 1|$

$$L(\omega) = \begin{cases} |1 - \cos\omega|, & \text{if } \dfrac{\pi}{2} < \omega \leq \dfrac{3\pi}{2} \\ |1 + \cos\omega|, & \text{otherwise} \end{cases}. \tag{2.31}$$

If we let the bottommost ray be $\mathcal{N} = 1$ and the topmost ray be $\mathcal{N} = 100$, then the position of the ith ray is

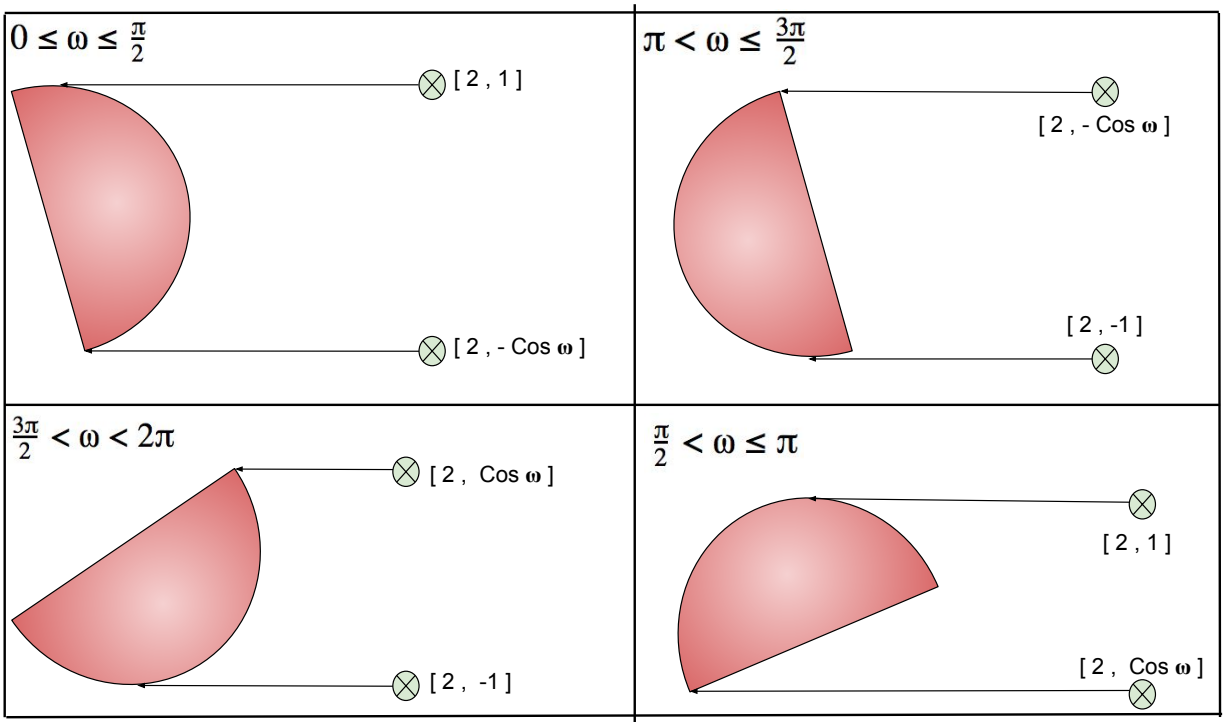

Figure 2.9: The x and y positions of the topmost and bottommost ray that would intersect the semicylinder for the four rotation regimes. When we simulate this system in the *Mathematica* module, these are the $\vec{r}_{ray}$'s we'll use.

$$\vec{r}_{ray,i} = [2, \Delta x(i-1)] = [2, \frac{L}{99}(i-1)].$$

Now we only need to set the power of the rays, Φ_{ray}, such that we are approximating a plane wave with $I = 1\ \frac{Watt}{m^2}$. Consider the flat side to have a length $\mathcal{L} = 2\ m$ and imagine the cylinder to have a height $h = 1\ m$ in the $\hat{z}$ direction. We should have the total power $\Phi_{tot} = \mathcal{L}\ h\ I = 2\ Watts$. Since we have 100 rays, each ray should have a power of

$$\Phi_{ray} = \frac{\Phi_{tot}}{100} = \frac{1}{50}\ Watts. \tag{2.32}$$

The Φ_{ray} we just derived is only valid for $\omega = 0$, and so we need to find Φ_{ray} for an arbitrary ω. Following the method laid out in the preceding paragraph, $\Phi_{tot} = L(\omega)\ h\ I$, and so

$$\Phi_{ray} = L(\omega)\ \frac{1}{100}\ Watts.$$

Now we have everything we need to apply the raytracing procedure to find the torque about the center of mass of the reflective semicylinder.

Fig 2.10. includes a plot of $c\ \tau_z$ as determined via the procedure outlined in the preceding section at $\omega = \frac{\pi}{40}$ intervals and the analytic solution (Fig 2.8) underlying in red. The numeric raytracing procedure is remarkably close to the exact value of the torque. There is some discrepancy as $\omega \longrightarrow \pi$ and $\omega \longrightarrow -\pi$, which is due to most of the rays intersecting the flat portion of the semicylinder. Since the rays that intersect the flat portion contribute no net torque, fewer rays will hit the relevant curved portion and thus decrease accuracy. Despite this, the net discrepancy is small and we can continue on to less trivial systems.

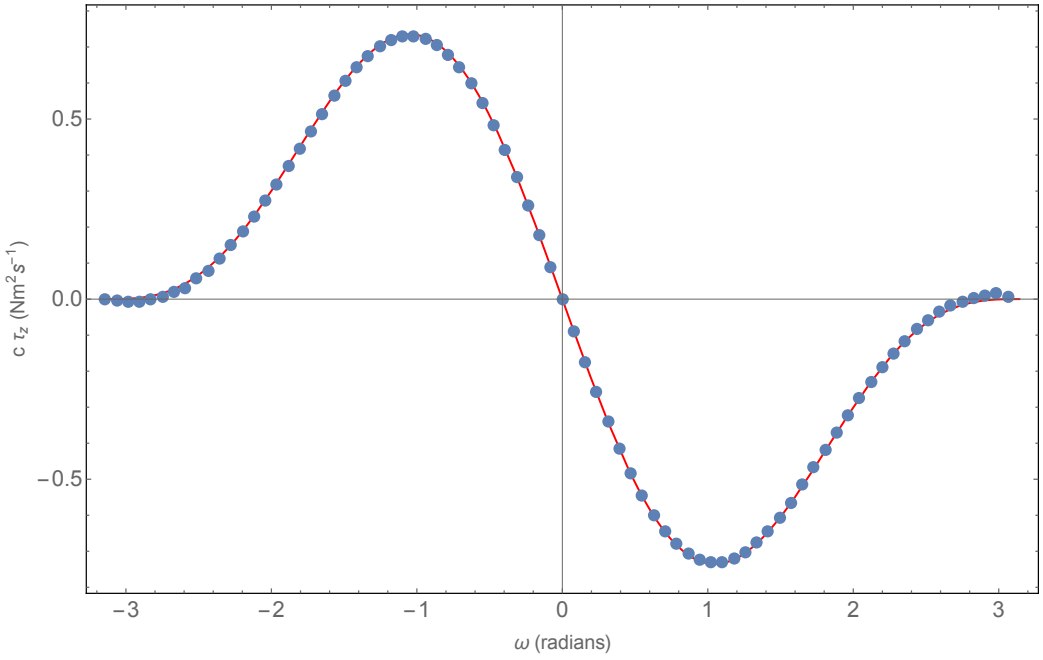

(a)

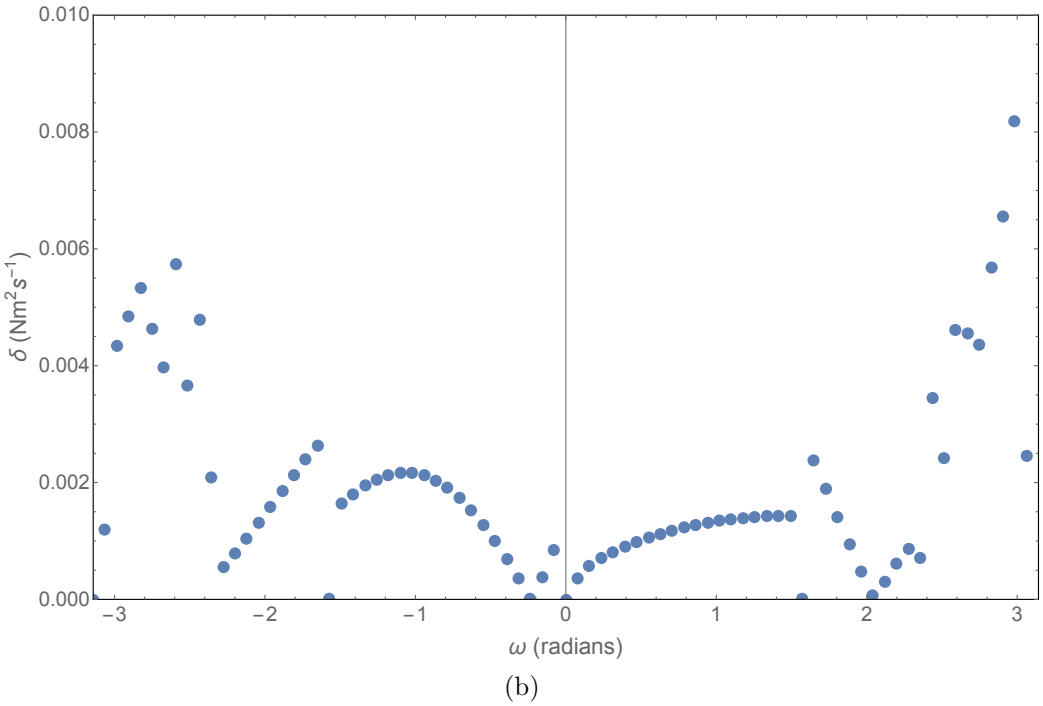

(b)

Figure 2.10: (a) A comparison of the analytic solution (in red) and the torque measured by the numeric ray tracing procedure as a function of ω. (b) The discrepancy, δ, between the analytic and numeric solution as a function of ω.

Chapter 3

Results

3.1 Torque and Forces

Now that we have shown that the ray tracing procedure is accurate, at least for the reflective semicylinder case, we can apply it to systems that involve transmission. Consider a semicylinder with index of refraction $n_{material}$. We apply the ray tracing procedure to this system with the same format as the reflective semicylinder case:

Parameter	Value
Number of Rays	100
Max N_{int}	3
$\vec{r}_{ray,i}$	$[-2, \frac{L(\omega)}{99}(i-1)]$
$\vec{k}$	$[1, 0]$
Φ_{ray}	$\frac{L(\omega)}{100}\frac{Nm}{m^2 s}$
B	False

Since $\vec{k} = [1, 0]$, the rays will come from the left rather than the right as depicted in the previous chapter. This is due to the *Mathematica* code being specifically designed for the rays to come from the left. This will have no effect on the calculations as long as we still rotate the semicylinders in the counterclockwise direction. Af-

ter three interactions, the average power of rays that are still within the body are $\Phi_{average} \approx .02\ \Phi_{initial}$[1]. In Fig 3.1 we plot the resulting torque for $n_{material} = 1.2$, 1.31, 1.4, 1.5, 2.42, and 10.

We note that a peculiar phenomenon occurs as the index of refraction increases. When $n < 1.3$, there are four stable angles of attack at $\omega \approx \pm 1.35$ & $\omega \approx \pm .85$ that result in a nonzero lift force, but this drops to two when $n > 1.3$. In addition, we note that $\omega = 0$ is unstable ($\frac{d\tau_z}{d\omega} > 0$) for a sufficiently low index of refraction, but becomes stable somewhere around and above $n \approx 1.31$. It is also important to note that for the $n = 2.42$ and 10 case, we didn't seem to consider enough rays to get accurate behavior around $\omega = \pi$. However, it's still apparent that there are only two stable, non-zero lift configurations for $n = 2.42$ at $\omega \approx \pm 1.754$ and none for $n = 10$.

The stable angles of attack, ω_i, where $\omega \neq 0$ are listed below.

$n_{material}$	ω_1	ω_2	ω_3	ω_4
1.2	-1.354	-.8504	.8509	1.351
1.31	-1.392	1.390	/	/
1.4	-1.439	1.440	/	/
1.5	-1.49	1.487	/	/
2.42	-1.753	1.754	/	/
10	/	/	/	/

Table 3.1: Stable angles of attack for transparent semicylinders with a constant index of refraction $n_{material}$. "/" represents the lack of a stable angle of attack.

Naturally, we want to know what these configurations look like in order to enhance our intuition regarding lightfoils, and some semicylinders at their ω_1 angle of attack are visualized in Fig 3.2. Overall, there doesn't seem to be any visual indication that the selected rotation angles are in any way a stable configuration.

[1]Even though this is dependent on $n_{material}$, nearly every value of $n_{material}$ will result in a Φ_{ray} around this range

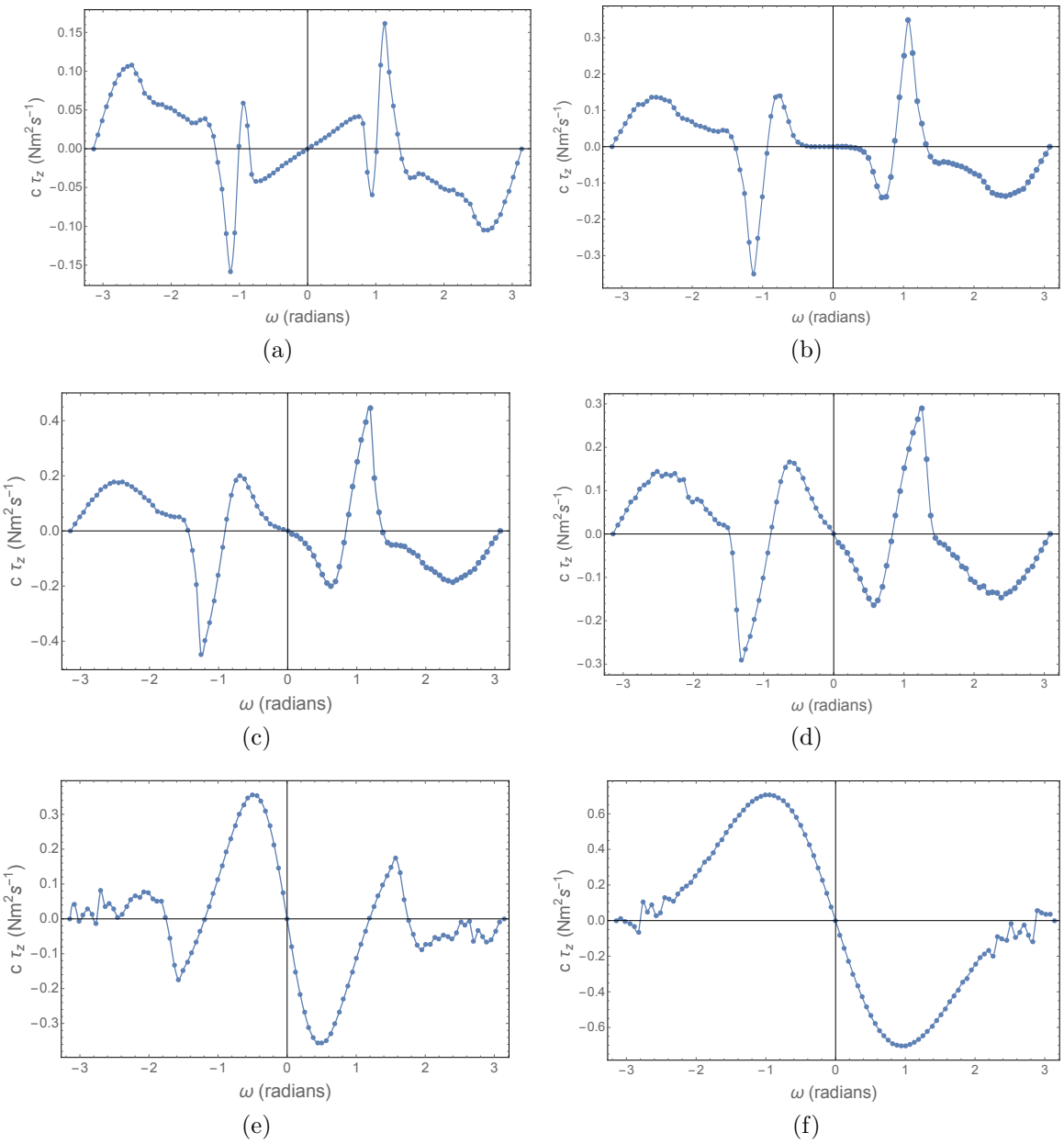

Figure 3.1: The torque output of our *Mathematica* module vs. the angle of rotation ω for (a) $n_{mat} = 1.2$, (b) $n_{mat} = 1.31$, (c) $n_{mat} = 1.4$, (d) $n_{mat} = 1.5$, (e) $n_{mat} = 2.42$, and (f) $n_{mat} = 10$. The module calculates the torque at $\frac{\pi}{50}$ intervals and all of the data is connected via a spline interpolation.

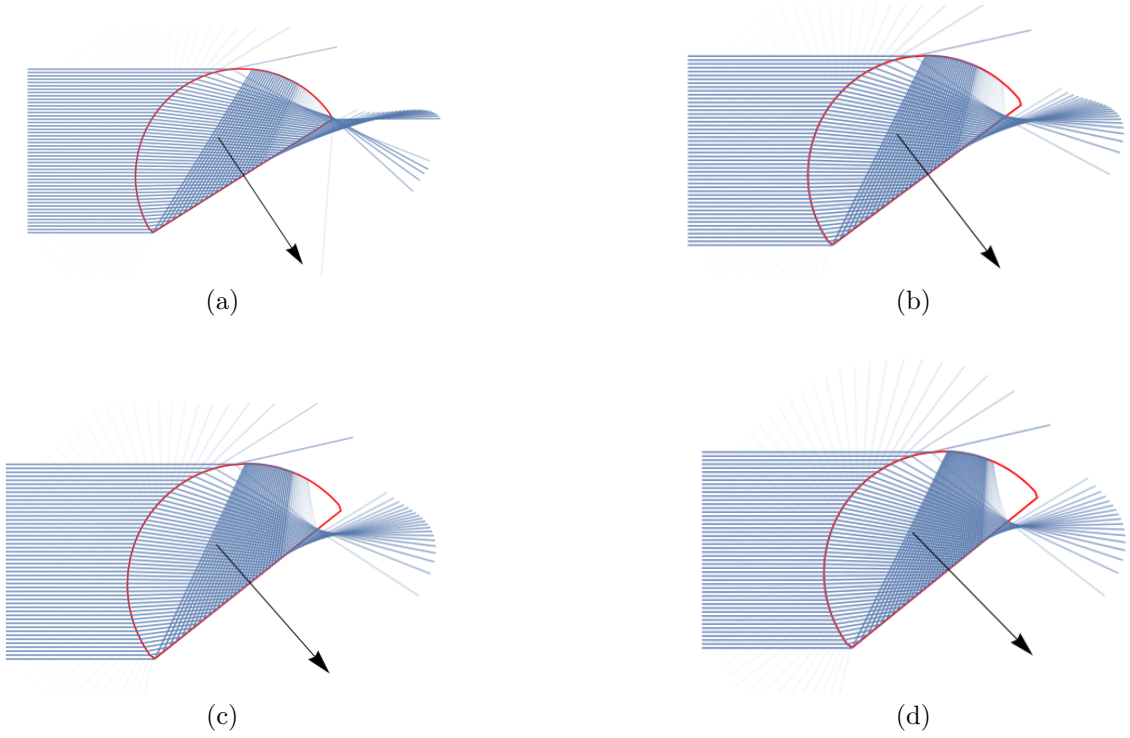

(a) (b)

(c) (d)

Figure 3.2: The semicylinders at their ω_1 stable angles of attack (see table 3.1) with (a) $n_{mat} = 1.2$, (b) $n_{mat} = 1.31$, (c) $n_{mat} = 1.4$, and (d) $n_{mat} = 1.5$. The direction of the net force on the body is shown by the black arrow, which demonstrates that a lift force is generated.

3.1.1 Dynamics

Let $\tau(\omega)$ be the spline interpolation of the z-component of the torque on the semicylinder at a rotation angle ω. As such, we can apply Newton's second law for rotation to the system,

$$\mathcal{I}\ddot{\omega} = \tau(\omega), \tag{3.1}$$

where $\mathcal{I}$ is the moment of inertia about the center of mass. Solving for ω in Eq. 3.1 will yield oscillatory solutions due to the periodic nature of $\tau(\omega)$ and because Eq. 3.1 conserves total mechanical energy. To make this solution more interesting, we adjust Eq. 3.1 with a damping factor γ:

$$\mathcal{I}\ddot{\omega} = \tau(\omega) - \gamma\ \dot{\omega}. \tag{3.2}$$

The damping factor seeks to approximate the torque a rotating body in a fluid would experience. We can apply a numeric ordinary differential equation solver to Eq. 3.2. The moment of inertia for a semicylinder[2] is $\mathcal{I} = (\frac{1}{2} - \frac{16}{9\pi^2})MR^2$, where M is the mass and R is the radius of the semicylinder. Swartzlander's paper experimented with semicylinders of radius $R = 10\mu m$, but the paper doesn't report on their mass. Assuming Swarzlander used borosilicate glass,where $\rho = 2590\frac{kg}{m^3}$ is the density of borosilicate glass, and given that the height of the cylinders are $h = 50\mu m$, the moment of inertia of the cylinders is

$$\mathcal{I} = 6.40 \times 10^{-22}\ (\text{kgm}^2). \tag{3.3}$$

We'll substitute the $\mathcal{I}$ determined in Eq. 3.3 into Eq. 3.1 for the following calculation. Fig 3.3 shows the angle ω as a function of time with $\gamma = 10^{-11}\ \frac{\text{kgm}^2}{\text{s}}$ (and $\gamma = 0$ in Fig. 3.3(f)) for various indices of refraction.

[2]A derivation of the moment of inertia for a semicylinder is given in the appendix

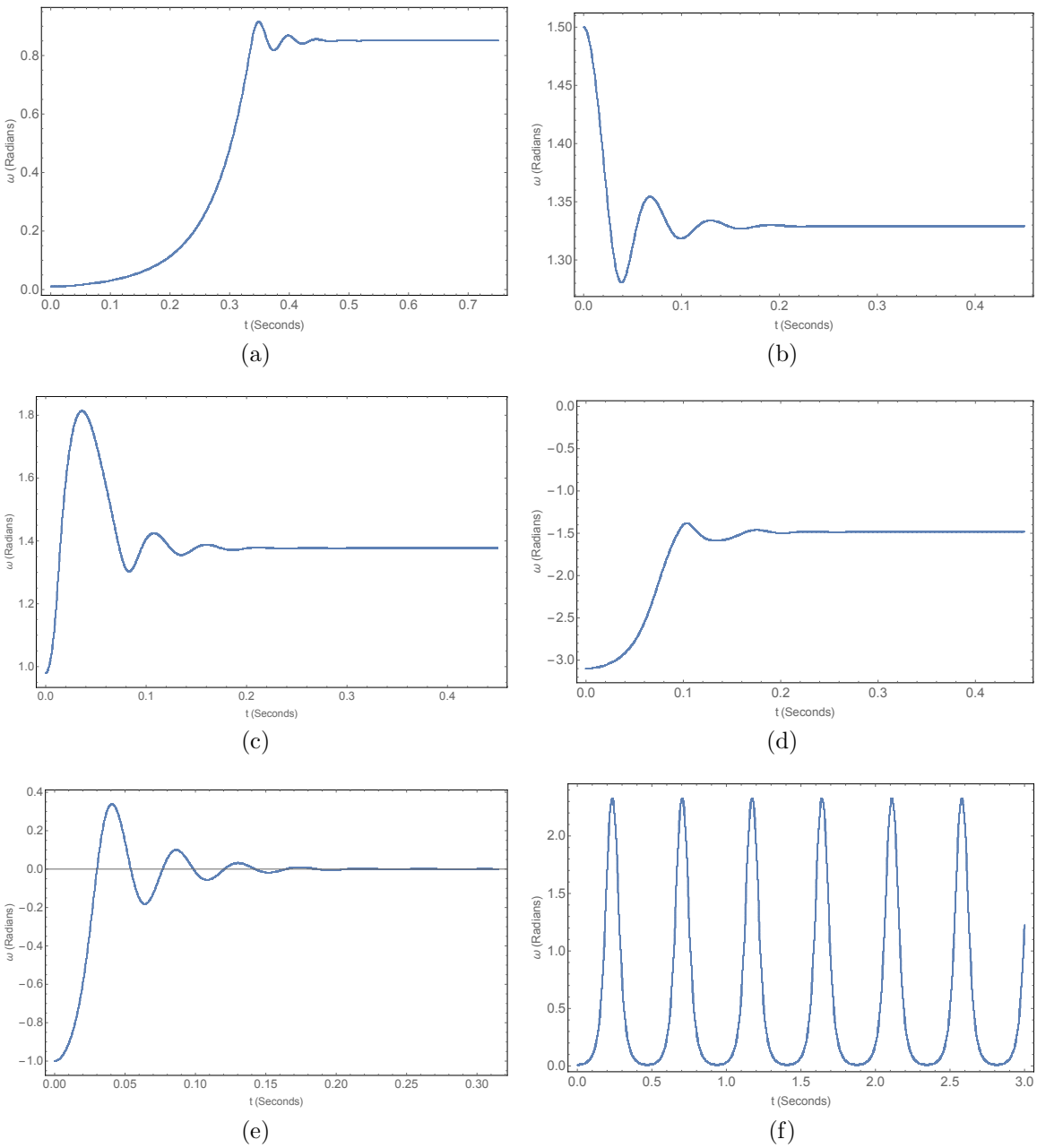

Figure 3.3: Various numeric calculations of the angle of rotation ω as a function of time with $\gamma = 10^{-11}\frac{\text{kgm}^2}{\text{s}}$ (unless otherwise stated) in the case of (a) $n_{material} = 1.2$, $\omega(0) = .5$, $\dot{\omega}(0) = 0$ (b) $n_{material} = 1.31$, $\omega(0) = 1.5$, $\dot{\omega}(0) = 1$ (c) $n_{material} = 1.4$, $\omega(0) = .98$, $\dot{\omega}(0) = 0$ (d) $n_{material} = 1.5$, $\omega(0) = -3.1$, $\dot{\omega}(0) = 0$ (e) $n_{material} = 2.42$, $\omega(0) = -1$, $\dot{\omega}(0) = 0$ and (f) the undamped case: $\gamma = 0$, $n_{material} = 1.2$, $\omega(0) = .01$, $\dot{\omega}(0) = 0$.

It is apparent that setting $\gamma = 10^{-11} \frac{\text{kgm}^2}{\text{s}}$ results in an underdamped system, but there is no specific reason that a damped lightfoil system has to be underdamped. Another important consideration is that we assumed the same power is hitting these micro-semicylinders as the semicylinder of $\mathcal{L} = 2$ m with $I = 1 \frac{\text{Watts}}{\text{m}^2}$. This would require an immensely powerful light source[3], but the main takeaway from Fig 3.3 is that the transparent semicylinders modeled in Fig 3.1 will rotate into a stable angle of attack regardless of the initial conditions. This isn't particularly surprising, but gives a sense of the mechanics of micrometer scale semicylinders in a fluid.

Consider the stable angles displayed in Table 3.1. While we've illustratively shown that these semicylinders exhibit optical lift, we can also quantify these lift forces. We'll use our ray tracing procedure to determine the net optical force on the semicylinders at each of the stable angles to show that they exhibit optical lift. Fig 3.4 shows the y-component of the optical force at ω_1 (see Table 3.1) vs. the index of refraction. We see that $n_{material} = 1.2$ exhibits the largest lift force of those studied, but we lack the data points necessary to find the full relation between F_y and n.

[3]If the source is still a plane wave, then $I \approx 10^5 \frac{\text{Watt}}{\text{m}^2}$

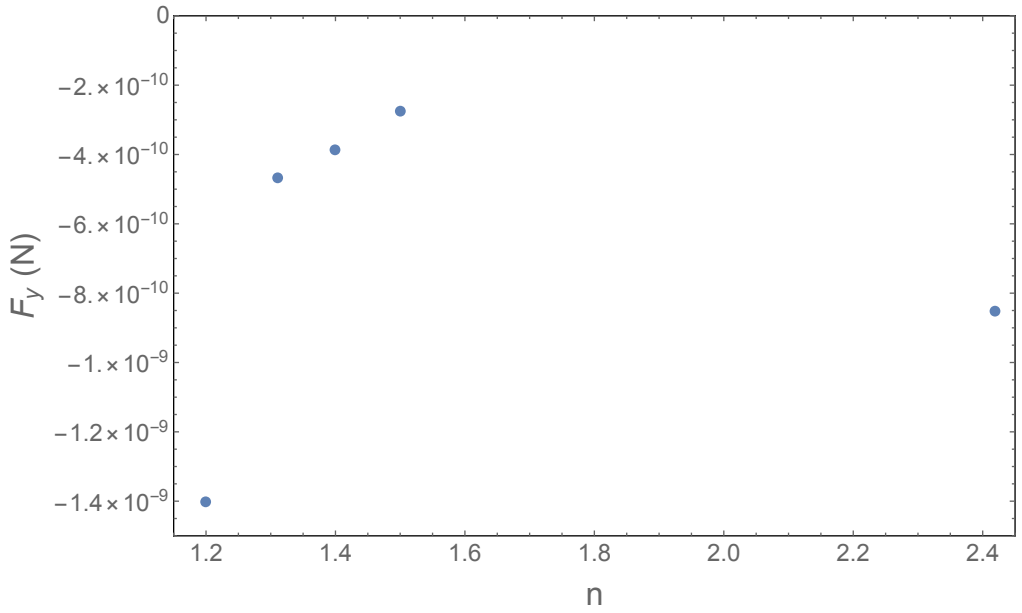

Figure 3.4: The magnitude of the optical force in the y-direction at stable angle ω_1 vs. the index of refraction.

Future Work

This topic is, by its nature, open-ended and there is no limit to the potential optical wing configurations that can be modeled. Future generations may have the opportunity to apply the procedure we've outlined in Chapter 2, and use it to find the optical forces on an airfoil, an ellipse, etc. Additionally, we can imagine that a lightfoil might be illuminated by a spherical rather than a plane wave. That would require a more rigorous procedure to determine the new optical forces, but it is certainly not impossible.

Appendix A

Mathematica Code

A.1 Generate Rays

In[32]:=
```
Rays[n_] := Table[{0, 0, {1, 0}, 1, False}, {p, 1, n}];
(* {raynum,position,direction,intensity,Flip n's?} *)

Raypositions[n_, Leng_, xstart_, α_] := Module[{i, new},
   new = Rays[n];
   For[i = 0, i < Length[new], i = i + 1,
    new[[i + 1, 2]] = {-xstart, -Leng / 2 + i * Leng / (Length[new] - 1)};
    new[[i + 1, 3]] = N[RotationMatrix[α].new[[i + 1, 3]]];
    new[[i + 1, 2]] = N[RotationMatrix[α].new[[i + 1, 2]]];
   ];
   Return[new];
  ];
```

A.2 Find Intersection between Ray and Surface

```
In[38]:= Propogate[Raylist_, F_] :=
  Module[{Intersection, xprop, DFX, DFY, ypos, xpos, i, p, pp, xdir, ydir, FFF,
    yprop, FF, intersect},
   xdir = Table[Raylist[[i, 3, 1]], {i, 1, Length[Raylist]}];
   ydir = Table[Raylist[[i, 3, 2]], {i, 1, Length[Raylist]}];

   xpos = Table[Raylist[[i, 2, 1]], {i, 1, Length[Raylist]}];
   ypos = Table[Raylist[[i, 2, 2]], {i, 1, Length[Raylist]}];

   xprop[x_] := Table[xpos[[i]] + xdir[[i]] * x, {i, 1, Length[Raylist]}];
   yprop[x_] := Table[ypos[[i]] + ydir[[i]] * x, {i, 1, Length[Raylist]}];

   FF[x_] := Table[F[xprop[x][[i]], yprop[x][[i]]], {i, 1, Length[Raylist]}];
   intersect = Table[0, {i, 1, Length[Raylist]}];
   For[i = 1, i ≤ Length[Raylist], i ++,
    p[x_] := FF[x][[i]];
    pp[x_] := D[p, x];
    intersect[[i]] = RootFind[p];
   ];



   Intersection = Table[{xprop[intersect[[i]]][[i]], yprop[intersect[[i]]][[i]]},
     {i, 1, Length[intersect]}];

   Return[Intersection];
  ];
```

A.3 Change in Direction for Reflected and Transmitted Ray

```
RayRefract[Intersects_, PrevRays_, F_, n1_, n2_] :=
  Module[{a, θts, NewRays, i, prevα, normal, θincident, na, nb, θt, b,
    TransmissionVector},
   NewRays = Rays[Length[Intersects]];
   (* New rays start at intersect of previous rays *)
   For[i = 1, i ≤ Length[NewRays], i ++,
    NewRays[[i, 2]] = Intersects[[i]];
    NewRays[[i, 1]] = PrevRays[[i, 1]] + 1;
   ];

   For[i = 1, i ≤ Length[Intersects], i ++,

    normal = Normalize[{Derivative[1, 0][F][Intersects[[i, 1]], Intersects[[i, 2]]],
       Derivative[0, 1][F][Intersects[[i, 1]], Intersects[[i, 2]]]}];
    b = -normal.PrevRays[[i, 3]];
    If[b < 0,
     normal = -normal;
    ];
    If[PrevRays[[i, 5]],
     na = n2;
     nb = n1,
     na = n1;
     nb = n2;
    ];
    b = -normal.PrevRays[[i, 3]];
    a = (na/nb)^2 (1 - b^2);
    TransmissionVector = na/nb PrevRays[[i, 3]] + (na/nb b - Sqrt[1 - a]) * normal;
    NewRays[[i, 4]] = (1 - R[PrevRays[[i]], normal, na, nb]) * PrevRays[[i, 4]];
    NewRays[[i, 3]] = TransmissionVector;
    If[PrevRays[[i, 5]],
     NewRays[[i, 5]] = False,
     NewRays[[i, 5]] = True;
    ];
   ];
   Return[NewRays];
  ];
```

In[42]:=
```
RayReflect[Raylist_, F_, n1_, n2_] :=
  Module[{Intersect, i, na, nb, normal, b, ReflRays, θc},
   Intersect = Propogate[Raylist, F];
   ReflRays = Rays[Length[Intersect]];

   For[i = 1, i ≤ Length[Raylist], i ++,
    ReflRays[[i, 2]] = Intersect[[i]];
    ReflRays[[i, 1]] = Raylist[[i, 1]] + 1;
    normal = Normalize[{Derivative[1, 0][F][Intersect[[i, 1]], Intersect[[i, 2]]],
       Derivative[0, 1][F][Intersect[[i, 1]], Intersect[[i, 2]]]}];
    b = -normal.Raylist[[i, 3]];
    If[b < 0,
     normal = -normal;];
    b = -normal.Raylist[[i, 3]];
    If[Raylist[[i, 5]],
     na = n2;
     nb = n1,
     na = n1;
     nb = n2;
    ];
    ReflRays[[i, 3]] = Raylist[[i, 3]] + 2 (b) * normal;
    ReflRays[[i, 5]] = Raylist[[i, 5]];
    ReflRays[[i, 4]] = R[Raylist[[i]], normal, na, nb] * Raylist[[i, 4]];
   ];
   Return[ReflRays];
  ];
```

A.4 Force of Rays on Surface

```
ForceTrace[Rays_, F_, n1_, n2_, InteractionLimit_] :=
 Module[{Forces, newRays, intersects, i, intnum, TheRays, Intersect, normal,
   Cosθ, na, nb, Cosθt, Force, PoweR, c},

  Forces = {};
  newRays = RayTrace[Rays, F, n1, n2, InteractionLimit];
  intnum = 0;
  While[intnum ≤ InteractionLimit,
   TheRays = RaySort[newRays, intnum];
   intersects = Propogate[TheRays, F];
   For[i = 1, i ≤ Length[RaySort[newRays, intnum]], i ++,
    TheRays = RaySort[newRays, intnum];
    Intersect = intersects[[i]];
    PoweR = TheRays[[i, 4]];
    c = 3 * 10 ^ 8;

    normal = Normalize[{Derivative[1, 0][F][Intersect[[1]], Intersect[[2]]],
       Derivative[0, 1][F][Intersect[[1]], Intersect[[2]]]}];

    Cosθ = -TheRays[[i, 3]].normal;
    If[Cosθ < 0,
     normal = -normal;
     Cosθ = -Cosθ;
    ];

    If[TheRays[[i, 5]],
     na = n2;
     nb = n1,
     na = n1;
     nb = n2;
    ];
    If[na > nb && ArcCos[Cosθ] >= ArcSin[n1 / n2],
     Cosθt = 0,
     Cosθt = Sqrt[1 - (na/nb)^2 (1 - Cosθ^2)];
    ];
    Force =
     PoweR/c (nb * Cosθt (1 - R[TheRays[[i]], normal, na, nb]) -
        na * Cosθ (1 + R[TheRays[[i]], normal, na, nb])) * normal;
    AppendTo[Forces, {Force, Intersect}];
   ]; intnum = intnum + 1;
  ]; Return[Forces];]

RayTorque[ForceList_, CoM_] := Module[{Force, Torque, r},
   r = Table[Append[ForceList[[i, 2]] - CoM, 0], {i, 1, Length[ForceList]}];
   Force = Sum[ForceList[[i, 1]], {i, 1, Length[ForceList]}];
   Torque = Sum[Cross[r[[i]], Append[ForceList[[i, 1]], 0]],
     {i, 1, Length[ForceList]}];
   Return[{Force, Torque[[3]]}];
  ];
```

A.5 Extra Information

The full *Mathematica* module with readme is available on my github via Robdei/RobbyRay.

Appendix B

Center of Mass of a Semicylinder

Consider the system laid out in Fig 2.5. We'll assume that the semicylinder is of homogeneous composition. Let σ be the mass area density of the semicylinder,

$$\sigma = \frac{2\ M}{\pi\ R^2},$$

where M is the total mass of the system and R is the radius of the semicylinder. We define the mass of an infinitesimal area element, dm, as

$$dm = \sigma\ r\ d\theta dr$$

where r is the distance of the area element from the origin. Since the semicylinder is bilaterally symmetric about the line $x = 0$, we know that the y-component of the the center of mass, CoM_y, is zero.

The x-component of the center of mass, CoM_x, is given by

$$CoM_x = \frac{1}{M}\int_0^M \vec{r}\cdot\hat{x}\ dm = \frac{\sigma}{M}\int_{-\frac{\pi}{2}}^{\frac{\pi}{2}} \cos\theta d\theta \int_0^R r^2 dr,$$

Where $\vec{r}$ points from the center of the circle to the mass element dm. This simplifies

to

$$CoM_x = \frac{2\ R}{3\ \pi} \int_{-\frac{\pi}{2}}^{\frac{\pi}{2}} \cos\theta d\theta = \frac{4\ R}{3\ \pi}.$$

Appendix C

Moment of Inertia of a Semicylinder

Consider the system detailed in Fig 2.5. From Appendix B, the mass area density is

$$\sigma = \frac{2\ M}{\pi\ R^2},$$

and the mass of an infinitesimal area element is

$$dm = \sigma\ r\ d\theta dr.$$

Lets compute the moment of inertia for a semicylinder about the center of the circle. The moment of inertia of an object is defined as

$$\mathcal{I} = \int r^2 dm,$$

and so the moment of inertia of a semicylinder about its center is

$$\mathcal{I}_0 = \frac{2M}{\pi R^2} \int_{-\pi/2}^{\pi/2} d\theta \int_0^R r^3 dr$$

or

$$\mathcal{I}_0 = \frac{1}{2}MR^2.$$

To find the moment of inertia about the center of mass, $\mathcal{I}_{CoM}$, we apply the parallel axis theorem:

$$\mathcal{I}_{CoM} = \mathcal{I}_0 - M\left(\frac{4R}{3\pi}\right)^2 = \left(\frac{1}{2} - \frac{16}{9\pi^2}\right)MR^2.$$

References

[1] J. Maxwell, *A Treatise On Electricity And Magnetism* (Oxford University Press, 1871).

[2] E. Nichols and G. Hull, "The Pressure Due To Radiation," Astrophysics **16** (1903).

[3] A. Guess, "Poynting-Robertson Effect for a Spherical Source of Radiation," Astrophysical Journal (1962).

[4] E. Hecht, *Optics* (Pearson, 2017), 5th ed.

[5] K. Neumann and S. Block, "Optical trapping," AIP **75** (2004).

[6] G. Swartzlander, T. Peterson, A. Artusio-Glimpse, and Raisanen, "Stable Optical Lift," Nature Photonics **5**, 48 (2010).

[7] D. Griffiths, *Introduction to Electrodynamics* (Pearson, 2016), 4th ed.

[8] M. Burt and R. Peierls, "The Momentum of a Light Wave in a Refracting Medium," Royal Society **333** (1973).

[9] L. Zhang, W. She, N. Peng, and U. Leonhardt, "Experimental evidence for Abraham pressure of light," New Journal of Physics **17** (2015).

[10] T. Peterson, Master's thesis, Rochester institute of Technology (2011).

[11] R. Pfeifer, T. Nieminen, N. Heckenburg, and H. Dunlop, "Colloquium: Momentum of an electromagnetic wave in dielectric media," Reviews of Modern Physics (2007).

[12] J. Moran, *An Introduction to Theoretical and Computational Aerodynamics* (Dover Books, 1984).

[13] G. Spencer and M. Murty, "General Ray-Tracing Procedure," Optical Society of America **52**, 672 (1961).

[14] J. Franklin, *Computational Methods for Physics* (Cambridge University Press, 2013).

[15] B. Greve, "Reflections and Refractions in Ray Tracing," Stanford Press (2006).

[16] T. Pozar, "Oblique reflection of a laser pulse from a perfect elastic mirror," Optics Letters **39**, 48 (2013).

[17] P. Kinsler, "Four Poynting Theorems," IOP Publishing (2009).